



**POLITECNICO**  
MILANO 1863

SCUOLA DI INGEGNERIA INDUSTRIALE  
E DELL'INFORMAZIONE

# A meta-model based procedure for the assessment of impact forces of dry granular masses on rigid barriers

TESI DI LAUREA MAGISTRALE IN  
CIVIL ENGINEERING FOR RISK MITIGATION

Author: **Ali Ahmadi**

Student ID: 10764844

Advisor: Prof. Francesco Calvetti

Co-advisors:

Academic Year: 2023-24



# Abstract

A meta-model-based procedure has been grounded to assess the impact force of dry granular masses on rigid barriers. The main aim of this study is to predict the maximum impact forces by taking advantage of machine learning and interpreting the data to de-normalise, refine, and optimise the empirical formula eq.4 [12] for the assessment of impact forces of dry granular masses on rigid barriers that have uncertainties between parameters of the system. In this thesis, the main aim is to apply uncertainty quantification in the framework of UQLab to overcome the behaviour of complex systems [44]; therefore, meta-modelling is implemented to develop surrogate models that are capable of representing the behaviour of the system in the presence of uncertainties. Several meta-modelling techniques are implemented to enhance the accuracy of the prediction for the maximum impact forces and perform sensitivity analysis, offering valuable insight into the importance of the system parameters. Since the empirical formulae are polynomial eq.4, the meta-models in this study were built by taking advantage of polynomial chaos expansion with different computational methods. Since the meta-models cannot estimate the formula, the integration of maximum impact forces with the Polyfit function took place to obtain the maximum impact formula. This refinement reduced the errors and calibrated the empirical formulae.

**Keywords:** Meta-modelling, Impact forces, Dry granular masses, Uncertainty quantification, Sensitivity Analysis, Machine learning



## Abstract in lingua italiana

Un procedimento basato sul meta-modellazione è stato sviluppato per valutare la forza d'impatto delle masse granulari asciutte su barriere rigide. Lo scopo principale di questo studio è prevedere le forze d'impatto massime sfruttando il machine learning e interpretare i dati per denormalizzare, perfezionare e ottimizzare la formula empirica eq.4 [12] per la valutazione delle forze d'impatto delle masse granulari asciutte su barriere rigide, che presentano incertezze tra i parametri del sistema. In questa tesi, l'obiettivo principale è applicare la quantificazione dell'incertezza nel contesto di UQLab per superare il comportamento dei sistemi complessi [44]; pertanto, la meta-modellazione è implementata per sviluppare modelli surrogati capaci di rappresentare il comportamento del sistema in presenza di incertezze. Diverse tecniche di meta-modellazione sono implementate per migliorare l'accuratezza della previsione delle forze d'impatto massime e per eseguire l'analisi di sensibilità, offrendo preziose intuizioni sull'importanza dei parametri del sistema. Poiché le formule empiriche sono polinomiali eq.4, i meta-modelli in questo studio sono stati costruiti sfruttando l'espansione del caos polinomiale con diversi metodi computazionali. Poiché i meta-modelli non possono stimare la formula, l'integrazione delle forze d'impatto massime con la funzione Polyfit è avvenuta per ottenere la formula dell'impatto massimo. Questo perfezionamento ha ridotto gli errori e calibrato le formule empiriche.

**Parole chiave:** Meta-modelling, Forze d'impatto, Masse granulari asciutte, Uncertainty quantification, Analisi di sensitività, Machine learning



# Contents

<b>Abstract</b>	<b>i</b>
<b>Abstract in lingua italiana</b>	<b>iii</b>
<b>Contents</b>	<b>v</b>
<b>Introduction</b>	<b>1</b>
<b>1 Literature review</b>	<b>3</b>
1.1 DEM assessment of impact forces of dry granular masses on rigid barriers .	4
1.1.1 Impact Force Evaluation . . . . .	5
1.1.2 Description of dataset . . . . .	5
1.1.3 Range of parameters . . . . .	5
1.1.4 Empirical Equation for MIF . . . . .	6
1.2 A Meta-Model-Based Procedure for Quantifying the On-Site Efficiency of Rockfall Barriers (FE) . . . . .	10
<b>2 Methodology</b>	<b>13</b>
2.1 Definition of Meta-Modelling: . . . . .	13
2.1.1 Black-box definition: . . . . .	14
2.1.2 Training data set: . . . . .	14
2.2 Meta-Modelling different machines . . . . .	15
2.2.1 Polynomial Chaos Expansion (PCE): . . . . .	15
2.2.2 Support Vector Machine (SVM) . . . . .	17
2.2.3 Kriging . . . . .	17
2.2.4 Polynomial Chaos-Kriging (PC-Kriging) . . . . .	18
2.3 Sensitivity Analysis . . . . .	18
2.4 Bayesian inference and Probabilistic model . . . . .	19
2.4.1 Bayesian inference . . . . .	19

2.4.2	Probabilistic model . . . . .	19
2.5	Reliability . . . . .	20
<b>3</b>	<b>Traditional approach</b>	<b>21</b>
3.1	Maximum impact force action . . . . .	22
3.2	Dynamic contribution to the Impact force . . . . .	31
3.3	Normalisation of Maximum Impact Force ( $\Delta_{MIF^*}$ ) . . . . .	36
<b>4</b>	<b>Meta-modelling approach</b>	<b>43</b>
4.1	Probabilistic Model . . . . .	44
4.2	General overview of Polynomial Chaos Expansion with different computational methods: . . . . .	49
4.2.1	Sensitivity Analysis Sobol' Indices . . . . .	52
4.2.2	Meta-model based on Bayesian Compressive Sensing (BCS) . . . . .	55
4.3	Dynamic contribution to the Impact force . . . . .	65
4.4	Normalisation of Maximum Impact Force ( $\Delta_{MIF^*}$ ) obtained by meta-model	70
<b>5</b>	<b>Conclusions</b>	<b>77</b>
	<b>Bibliography</b>	<b>79</b>
	<b>A Reference for figure 35</b>	<b>85</b>
	<b>B Reference for figure 36</b>	<b>87</b>
	<b>List of Figures</b>	<b>89</b>
	<b>List of Tables</b>	<b>93</b>
	<b>List of Symbols</b>	<b>95</b>
	<b>Acknowledgements</b>	<b>97</b>

# Introduction

## Debris flow

The United States Geological Survey (USGS) considers it a type of rapid landslide, focusing on its fast-moving and destructive nature [28]. Debris flows are characterised by destructive nature instinct [9, 21, 28, 33]. Debris flow is defined by various authors based on factors such as material type, water saturation, and mass velocity [9]. They might be triggered by heavy rainfall, flash floods or erosion and move substantial elements such as boulders, trees and even cars downhill [21] [28]. Debris flow is a non-homogeneous, solid-liquid two-phase flow between solid and liquid phases [51]. This flow is characterised by the energy of the liquid phase [57] and characterised by rheological factors such as viscosity and yield stress that determine its movement [40].

The characteristics of debris flows are complex, with their destructive ability to carry large boulders [21]. These flows are common in mountains and hills, where they locate a significant hazard to life and property [33] [9]. It is an intermediate phenomenon between hyperconcentrated flows and landslides, with two primary types: muddy and granular [17]. The impact of debris flow correlated to the properties of particles, gravity, discrete force from particle collision, and buoyant force created by high-volume mud [8].

## Dry Granular Masses of Debris Flow

Dry granular masses in debris flows exert significant impact forces on rigid barriers, which create hazards to the residential area [47] [13]. Impact forces are affected by various factors, such as flow length, height, front inclination, porosity and velocity [47]. The use of discrete element modelling is a way to understand the impact of granular debris flows on rigid structures. Although progress has been made in understanding the physics of debris flows, there is a demand for empirical methods in hazard assessment due to uncertainties in initial and boundary conditions [32].



# 1 | Literature review

The assessment of risk due to the landslide events include: The comprehension modelling of the hydromechanical processes developing when the landslide interacts with either civil structures or protection works. The aim of this topic on the dynamic impact of dry granular flows against protective barriers/ embankments, and in particular, it is aimed at estimating the maximum impact forces (MIF) exerted on these latter. To achieve this goal, the barrier is assumed to be rigid which allows us to uncouple and simplify the problem with the consequence of conservatively overestimating the impact forces. At present the classical approaches employed to design sheltering structures are commonly inspired to those used in case of:

Impact of fluid masses on rigid barriers. These models, which are aimed at estimating the pressures applied to the obstacles, can be thus subdivided in hydrostatic (HS) and hydrodynamic (HD). Impact of boulders (BI) on elastic walls. Hydrostatic models [3, 30, 31, 50, 52] have been extensively used for the last 30 years to estimate debris impact forces, even if they are quite simplistic. In these models, a linear pressure profile with depth is assumed, and impact force depends on flow height and debris unit weight only. In hydrodynamic models [2, 7, 29, 38, 42, 52, 58], a constant pressure profile is assumed, and impact force depends on impact mass velocity (in addition to the factors considered by hydrostatic models). On the other side, most common BI models [29, 38] consider elastic impacts and refer to the Hert's theory of contacts between two elastic spheres for evaluating impact force. In this case, the MIF mainly depends on the impact velocity, the elastic parameters of the impacting bodies, and the boulder mass. At last, hybrid models combine the above-mentioned fluid and solid-based models [2].

In general, the MIF values evaluated by means of hydraulic models provide lower bound values, whereas solid impact models upper bound values [29]. Analogous considerations on the comparison of the above-mentioned models are given in [30, 38].

All in all, the review of the literature clearly shows that as of today the design of sheltering structures has been tackled either theoretically or empirically, whereas the use of numerical codes for this purpose is not yet very common in practice. Due to uncertainty between

parameters application of meta-modelling techniques take place to observe the correlation of each parameter in our complex system for the impact forces of dry granular flows on rigid barriers emphasises the importance of considering different parameters in the design of protective structures such as shelters [12, 13, 15, 55] for better observation and understanding this complexity in the system.

### 1.1. DEM assessment of impact forces of dry granular masses on rigid barriers

The discrete Element Method (DEM) is used to obtain the impact force of dry granular flows on rigid barriers. This method has been implemented for the accurate tracking of the particle motion, which leads to understanding the factors that influence impact forces, such as flow velocity, mass, height, front inclination, void ratio, and the barriers properties [12, 13]. Moreover, the implementation of this method leads to study of complex granular flows, such as nonspherical, flexible, or cohesive particles, which is useful in providing particle stress information for the development of constitutive models [26]. The numerical simulations were performed using the PFC 3D code [18, 19]. The geometry of the model is shown in Figure 1, in which both granular assembly and wall elements represents the boundary and rigid barrier. In order to ease the progress, plane strain conditions are imposed by confining the model within two smooth lateral wall elements. The flow width is 8 times the average grain diameters  $D$ , therefore, the influence of the lateral boundary on the numerical results is negligible [11, 24]. The initial velocity of the granular mass is assigned at the instant of time just preceding the impact. The obstacle is assumed to be vertical, and the sliding plane is horizontal. The granular mass is modelled as a random assembly of spherical rigid grains. Following the approach proposed by Calvetti [10] for quantitative reproduction of soil behaviour, the model consists of spherical particles, and the rotation is inhibited to capture the effect of irregular shape of the soil particles.

These parameters include flow properties, material characteristic, and rigid barrier properties. Discrete Element Method (DEM) simulations are a valuable tool for the complex relationships between these factors and resulting impact forces, which provide more accurate and reliable design methodologies [12, 13, 16, 55].

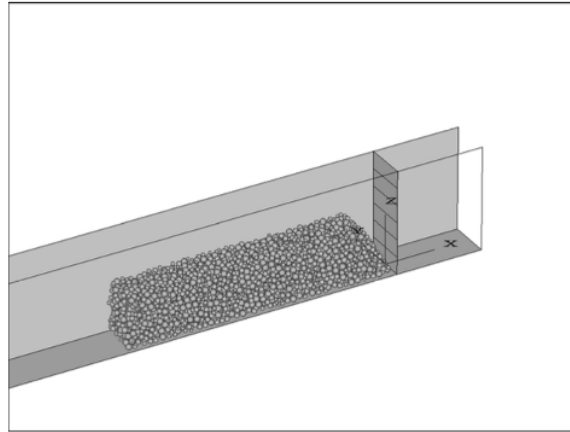


Figure 1: DEM model initial conditions

The key points of the document include:

### 1.1.1. Impact Force Evaluation

The evaluation of the impact forces in dry granular flows against barriers is important in the risk assessment and protection design. [12–14] studied the assessment of impact force by using 3D discrete element code to model the impact process in order to obtain a design formula. However, the assumption of a rigid barrier leads to an overestimation of impact forces.

### 1.1.2. Description of dataset

In this experiment, a variety of variables were defined to analyse the maximum impact force of dry granular masses on rigid barriers. The model designed for the average grain diameter ‘D’ and the width of the grain assembly or width of our model ‘b’ equal to 8 diameters of grains, the length of grain assembly ‘l’, the height of grain assembly is ‘h’, the height of the barrier,  $\gamma_s$   $25.5kN/m^3$  unit weight of particles were used to normalised the maximum impact forces (MIF) were calculated by PFC to obtain  $\Delta_{MIF*}$ , v is impact velocity the range is,  $\alpha$  is the front inclination h is the flow height and ‘n’ initial porosity.

### 1.1.3. Range of parameters

A range of parameters were used in the simulations, and the average diameter ‘D’ is 0.3m. The ratio between the largest and smallest diameters is 2.4, ‘n’ initial porosity range is between 0.45 and 0.65 ( 0.45 picked for the simulation), and the range of the length of

the grain assembly 'l' is between 2.5 and 80 m (15m picked). The width of the grain assembly 'b' is 8 times the diameter of the grain 2.4m, the height of the grain assembly is between 1.5m and 7.5 (3m picked), the inclination of the front  $\alpha$  is between  $60^\circ$  and  $90^\circ$  with the  $10^\circ$  interval, the height of obstacle is 9m, total mass  $m(t)$  range is between 25-1200 (154 picked), the number of grains is 700-33'600 (4200 picked) and initial average velocity range is between 4 -128 (6,48 picked).

#### 1.1.4. Empirical Equation for MIF

The author (Calvetti et al. 2017) [12] provide a quantitative estimation for MIF derived from the interpretation of all numerical results obtained by considering the reference mechanical parameters, by imposing interparticle friction coefficient  $f_c$  was chosen 0.3, a typical value for DEM models of soils and by changing the front inclination, the flow height and Froud number within the following range  $\alpha = 60 - 90$ ,  $h = 1.5 - 7.5m$  and  $Fr = 0 - 14.4$ . All the results in terms of  $\Delta_{MIF^*}$  (normalised) versus Froud number are plotted in Figure 2; as previously observed,  $\Delta_{MIF^*}$  increases nonlinearly with  $Fr$  and larger values are obtained for smaller flow height  $h$ ; within each class of flow height,  $\Delta_{MIF^*}$  increases with the front inclination  $\alpha$ . For impact velocities tending to zero, the impact force should tend towards a static value, which is theoretically given by the passive thrust defined as:

$$S_p = \frac{1}{2}\gamma b h^2 k_p \quad (\text{eq.1})$$

Where,  $k_p$  and  $\gamma$  are the passive thrust coefficient and the unit weight of the equivalent continuum. Therefore, in order to highlight the dynamic contribution to the impact force, it is convenient to represent the numerical data by employing the new variables:

$$\Delta_{MIF} = MIF - S_p \quad (\text{eq.2})$$

Where,  $f_s$  stands for the impact force:

$$f_s = \frac{1}{2}\gamma_s b h^2 \quad (\text{eq.3})$$

Would be the static force exerted on a rigid barrier by fluid with a unit weight equal to the unit weight of the grains  $\gamma_s$ .

In which the total maximum is the departure of static contribution. All the values of  $\Delta_{MIF^*}$  obtained from the simulations are thus plotted in Figure 2 versus  $Fr$ , and there is the numerical data area also quite satisfactorily fitted by following the polynomial formula [13].

$$\Delta_{MIF^*} = a_1 F_{rM} Fr + a_2 Fr^2 \quad (\text{eq.4})$$

Where  $a_1$  and  $a_2$  are two non-dimensional coefficients, whereas  $F_{rM}$  is the intrinsic Froude number defined as:

$$F_{rM} = \frac{u_M}{\sqrt{gh}} \quad (\text{eq.5})$$

Where  $u_M$  is the velocity of propagation of compression waves within the impacting medium that in all cases here considered, corresponding to the same initial porosity, is approximately equal to 200 m/s. Note that, since  $u_M$  solely depends on the material stiffness and density,  $F_{rM}$ , for a given material depends only on  $h$ .

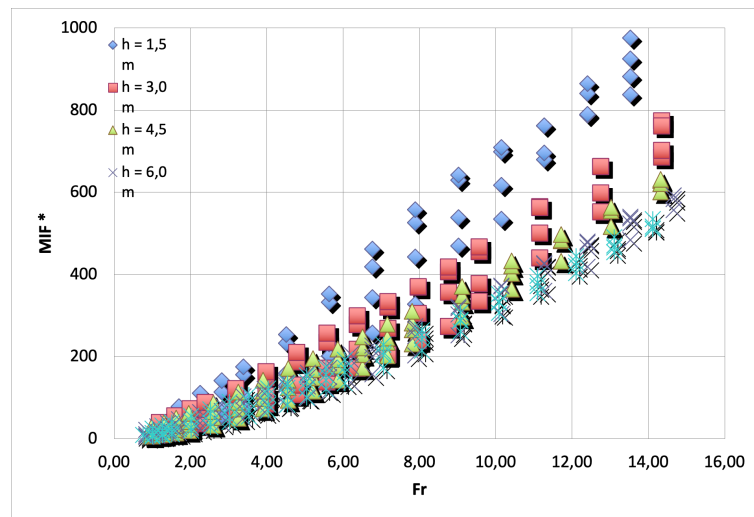


Figure 2:  $\Delta_{MIF^*}$  versus  $Fr$  ( $h=1.5-7.5$ )m  $\alpha = 60 - 90$ ; Reference Mechanical parameters

Table 1: Interpolation parameters  $a_1$  and  $a_2$  as a function of both front inclination and intrinsic Froude number

$\alpha$	$a_1$	$a_2$				
		$F_{rM} = 52$	$F_{rM} = 36.8$	$F_{rM} = 30$	$F_{rM} = 26$	$F_{rM} = 23.3$
-	-	$h = 1.5m$	$h = 3m$	$h = 4.5m$	$h = 6m$	$h = 7.5m$
60°	0.15	4.5	3	2.75	2.5	2.25
70°	0.4	3.5	2.75	2.5	2.25	2
80°	0.55	2.8	2.25	2	1.8	1.7
90°	1	1.3	1.25	1.1	1.05	1

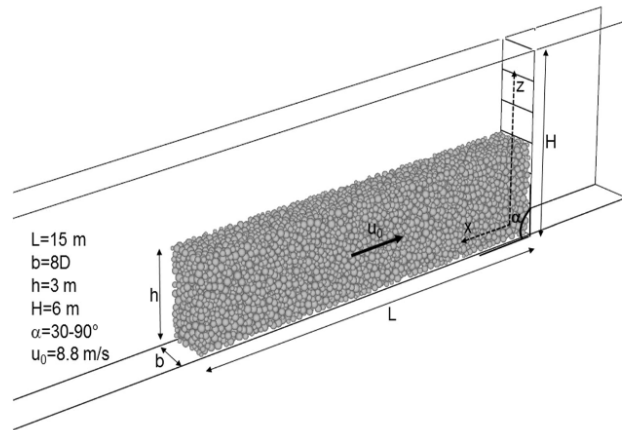


Figure 3: 3D view of the DEM model with test conditions

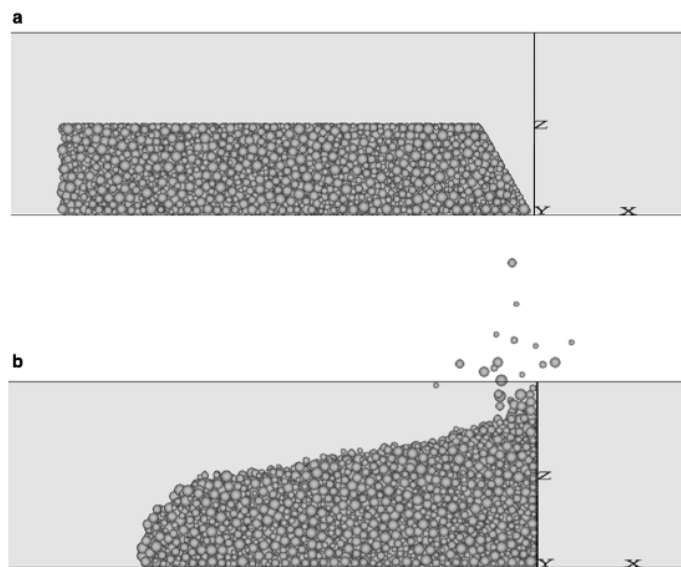


Figure 4: Reference test results a) initial configuration of the granular mass b) final configuration of the granular mass

## 1.2. A Meta-Model-Based Procedure for Quantifying the On-Site Efficiency of Rockfall Barriers (FE)

The aim of (Lambert et al., 2021) [39] is to develop a procedure for the efficiency in assessing the rockfall barriers in arresting the rock blocks. To achieve this, meta-modelling techniques are implemented, where a meta-model is a mathematical model that predicts the output of a complex numerical model. Once the meta-model has been trained, it can predict the barrier's performance for different input conditions. This information can be used to design more effective barriers for stopping blocks of different sizes and velocities. In [39], six different meta-modelling methods were used to determine the reliable approach.

The meta were used in this study:

**Meta1:** The method that combines regression trees to predict barrier response. It facilitates to handle of complex relationships between input parameters and barrier efficiency [35].

**Meta2:** Flexible Discriminant Analysis (FDA) is implemented in Meta2. It visualises the decision boundaries between successful and failed barrier cases, which helps in understanding critical factors influencing barrier performance [27].

**Meta3:** It utilises random forest. It is a powerful method for generating multiple decision trees and combining their prediction for improved accuracy and robustness [6].

**Meta4:** This method employs neural networks, a powerful machine learning technique that is capable of capturing nonlinear relationships [48].

**Meta5:** This is based on a Support Vector Machine (SVM) with a radial basis function kernel. [39] This study facilitates classifying barrier responses while maximising the separation between successful and failed cases [56].

**Meta6:** This method is an effective approach to handling high-dimensional input data and selecting critical parameters [27].

In summary of this work [39], implementing a meta-model is beneficial in predicting the performance of barriers for a wide range of input conditions. Meta-models are relatively quick and inexpensive to use, also can be used to identify the most critical factors that affect the performance of barriers, and can be used to optimise the design of the barriers. The Meta1, Meta2, Meta5, and Meta6 provide insight to understand the barrier's response, such as whether or not the block will be arrested. Meta 4 is implemented to predict the barrier's response to new input parameters. The meta-modelling approach is indeed very site-specific and dependent on the specific barrier and loading condition; it is still possible to develop a global standard for meta-models by focusing on the general principle and methodologies involved in the meta-modelling process. This standard could provide guidelines for selecting appropriate meta-modelling methods, defining relevant input parameters, and validating and evaluating the performance of meta-models. The results obtained by meta-models have accuracy with 94% , which makes it a powerful tool for quantifying the barrier's efficiency.



## 2 | Methodology

### 2.1. Definition of Meta-Modelling:

According to the general framework of uncertainty quantification introduced in [22, 53], a computational model can refer to a physical system, a set of assessment criteria or any other kind of workflow that propagates a set of input parameters to a set of output quantities of interest Figure 5.

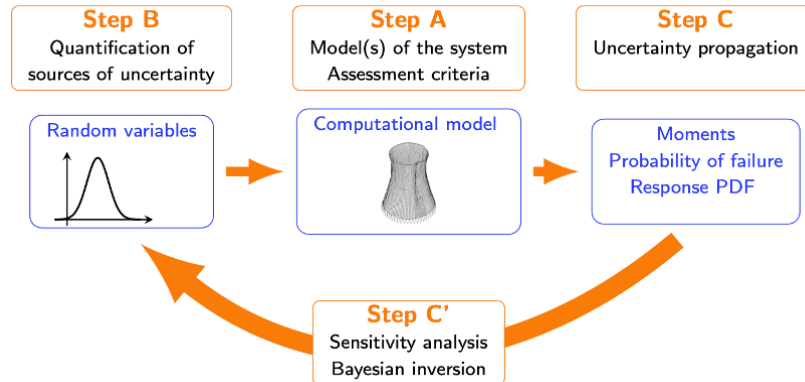


Figure 5: Visual representation of the global theoretical framework for uncertainty quantification developed by Sudret (2007); de Rocquigny et al. (2008), which gives the theoretical foundations to the UQLAB software.

Meta modelling is known as surrogate modelling or response surface, which is a statistical and mathematical technique used in experimental design in the field of modelling and simulation to approximate the behaviour of complex systems [4]. One of the main advantages of using meta-modelling is a cost-effective way to mimic the behaviour of the computational model. The most popular techniques for meta-modeling are based on parametric polynomial response surface approximations [4]. The term “meta” in meta-modeling refers

to the model being a model of another model, not the original model obtained by simulation or physical model. The implementation and procedure of meta-modeling are: Original Model: In many applications, creating a detailed and computationally expensive model in order to represent the behaviour of the system may not be practical due to time, resources, or computational constraints. This original model is referred to as the “black-box” model [44].

### 2.1.1. Black-box definition:

Black-box modelling is a method for approximating complex systems with low-complexity models. The construction of black-box models from input-output measurements without prior knowledge of the systems’s relationships with a focus on curve-fitting and statistical properties [41].

### 2.1.2. Training data set:

The meta-model is based on a set of training data, which consists of input-output data obtained from simulations or the original model. The meta-model “learns” from this data to create a mathematical representation of the system [44]. Applications: once the meta-model is produced and validated, it can be used for optimisation, sensitivity analysis or uncertainty quantification [44].

Advantages of using meta-modeling:

- **Computational Efficiency:**

Meta-models are much faster to evaluate and analyse compared with the original models, making them useful for tasks where repeated evaluations are necessary.

- **Global Understanding:**

Meta-models are able to provide insight into the relationship between input variables and model outputs, which helps in understanding the behaviour of the system.

- **Optimisation and Sensitivity Analysis:**

Meta models are often used in optimisation and sensitivity analyses in order to explore the design space efficiently. A variety of machines exist for implementing meta-models, including polynomial regression, Kriging (Gaussian process regression), neural networks, and radial basis functions. Meta modelling can be implemented in engineering, finance, and various scientific disciplines where complex models need to be predicted for efficient analysis and decision-making [44].

## 2.2. Meta-Modelling different machines

### 2.2.1. Polynomial Chaos Expansion (PCE):

It is a powerful meta-modelling tool which has important applications in uncertainty quantification and sensitivity analysis. Polynomial Chaos Expansion predicts the output of the model using a series expansion of orthogonal polynomials. Each term in the expansion is a product of a polynomial function of the input variables and coefficient. To obtain the PCE coefficient, the model is evaluated at a set of points, so-called the experimental design. The experimental design is typically generated using a space-filling algorithm such as Latin hypercube sampling.

### Computational methods

There exist various computational strategies and projection methods for determining the PCE coefficients:

- **Ordinary Least Squares-OLS:**

A regression method which minimises the sum of the squares of the differences between observed values and those values predicted by the model [44].

- **BCS- Bayesian Compressive Sensing:**

Bayesian inference utilises sparse signal recovery and is applied to PCE for identifying the most significant polynomial terms with a smaller number of model evaluations [44].

- **LARS- Least Angle Regression:**

A regression algorithm, which is similar to forward stepwise regression, moves the coefficient of the included variable towards its least squares value [44] instead of adding variables one by one.

- **OMP- Orthogonal Matching Pursuit:**

Orthogonal Matching Pursuit (OMP) is a greedy algorithm proposed [46] as a refinement of the Matching Pursuit algorithm [43]. OMP works by iteratively retrieving the polynomial basis elements that are most correlated with the current approximation residual and adding them to the active set of regressors [44].

- **Quadrature:**

A numerical integration method for computing and projecting the coefficient of the PCE by integrating the product of the polynomial terms with the input probability distributions [44].

- **SP- Subspace Pursuit:**

Subspace pursuit (SP) is a sparse regression algorithm developed by [20] and introduced for PCE by [23].

## Data distribution

For the distribution of the data, various distribution methods can be implemented, such as:

- **Uniform Distribution:**

Uniform distribution characteristics have a constant probability over a specified range, and all the values within the ranges have the same probability of occurring. The minimum and maximum values will define the range of parameters.

- **Beta Distribution:**

The beta distribution has a continuous probability distribution on the interval  $[0, 1]$ . It is used to model the distribution of random variables which represent probabilities.

- **Gamma Distribution:**

The Gamma distribution has a continuous probability distribution that is defined for the positive and real numbers [44]. It is used to model the time until the Poisson process reaches a certain count. Parameters: Shape parameter ( $k$ ) and scale parameter ( $\theta$ ).

- **Gaussian Distribution (Normal Distribution):**

The Gaussian distribution is known as the normal distribution and has a continuous probability of distribution. The main characteristic is that it is symmetric and bell-shaped, which is characterised by its mean and standard deviation. It is used in statistic and probability theory due to the Central Limit Theorem. Parameters: Mean ( $\mu$ ) and standard deviation ( $\sigma$ ).

### 2.2.2. Support Vector Machine (SVM)

Support vector machines are a class of learning techniques developed to solve problems by learning from examples. Such problems occur when one needs to approximate a function either because the latter is unknown, i.e. the underlying mapping is too complex to be modelled (e.g. meteorological phenomena) or because the function is too expensive to evaluate for practical purposes (e.g. finite element simulation). Classification is the specific case of supervised learning, which handles models whose outputs are discrete. Upon implementing the structural risk minimisation principle [56], support vector machine classification achieves a high degree of accuracy while minimising the risk of overfitting [44].

### 2.2.3. Kriging

Kriging (also known as Gaussian process modelling) is a statistical interpolation method that capitalises on Gaussian processes to interpolate a wide range of complex functions. It was first developed as a spatial interpolation tool in geostatistics by [36] and formalised by [45]. Kriging was later introduced in the context of metamodeling and computer experiments in the work [49], in which Kriging was used to represent an input/output mapping of an expensive computational model.

#### 2.2.4. Polynomial Chaos-Kriging (PC-Kriging)

Polynomial chaos kriging (PC-Kriging) is a novel metamodeling technique that combines the advantages of Kriging (Gaussian process modelling) and polynomial chaos expansions (PCE). More specifically, PC-Kriging consists of a universal Kriging model, the trend of which is modelled by a sparse set of orthogonal polynomials. UQLAB metamodeling tools provide an efficient, flexible and easy-to-use PC-Kriging module that allows one to apply state-of-the-art algorithms for different variations of PC-Kriging on a variety of applications [44].

### 2.3. Sensitivity Analysis

In general, sensitivity analysis aims to describe how the variability of the model response,  $y = M(x)$ , is affected by the variability of each input variable or combinations thereof. Sensitivity analysis is useful to spot unimportant input variables and help reduce the dimension of the problem (model reduction), among other usages. This kind of analysis is performed with a black-box approach, i.e. only based on the model response evaluations for a certain sample of inputs, selected in such a way that they will maximise the output information about the model structure [44]. These methods take into account the whole input domain. They may refer to different features of the model output, such as variance or distribution.

Below are various methods of sensitivity analysis:

- Borgonovo sensitivity indices [5]
- Sobol' sensitivity indices [1]
- Kucherenko sensitivity indices [37]

## 2.4. Bayesian inference and Probabilistic model

### 2.4.1. Bayesian inference

Bayesian methods [25] with a focus on inverse problems [34, 54]. An inverse problem arises when unknown parameters that cannot be directly measured are estimated based on experimental data that is only indirectly related to the parameters through a computational model. The problem is called inverse because instead of propagating information about input parameters through a computational model (so-called forward approach), the goal is to propagate information about the observations backward to obtain insight into the model inputs.

### 2.4.2. Probabilistic model

#### Probabilistic Input Model

In this step, the idea is to define the probabilistic model for the input parameters by defining the range of each input variable. These distributions represent the uncertainty associated with these parameters.

#### Sampling

The script generates random samples for the input parameters. by using different methods such as Monte Carlo, Latin Hypercube, Sobol, and Halton sampling. By using different types of methods such as Monte Carlo, Latin Hypercube, Sobol', and Halton, the random distribution of our data will be created.

Overall, the probabilistic approach is used to solve the problem of uncertainty. Probabilistic models are important for understanding and quantifying the uncertainties in the model's predictions or simulations. After obtaining new parameters for the input of the system, the output will be obtained by repeating the simulations based on the new input data to obtain enriched output.

The statistical distribution analysis of our inputs and the definitions of all the statistical approaches were defined briefly below:

- **Monte Carlo (MC):**

The Monte Carlo method is an algorithm for computation that depends on random sampling to obtain numerical results. The methods implemented to solve mathematical problems.

- **Latin Hypercube (LHS):**

Latin Hypercube Sampling is a statistical method that generates samples for multiple-dimension distribution. It guarantees an even and efficient coverage of the sample space in comparison with simple random sampling.

- **Sobol' series:**

Sobol series are quasi-random series that are implemented for numerical integration. Their usefulness in the design of an even coverage of the sample space than solely random sequences.

- **Halton Series:**

Halton series are another type of quasi-random sequence that aims to generate points into a space more even compared with random series. They are effective in low-dimensional spaces.

These methods are useful where traditional random sampling cannot provide sufficient coverage. Depending on the specific requirements and demands of the problem, researchers may choose one of these methods in order to improve the accuracy of their simulations.

## 2.5. Reliability

Structural reliability methods aim to assess the probability of failure of complex systems due to uncertainties associated with their design, manufacturing, environmental, and operating conditions. The name structural reliability comes from the emergence of such computational methods back in the mid-70s to evaluate the reliability of civil engineering structures. As these probabilities are usually small (e.g.  $10^{-2}$ ,  $10^{-8}$ ), this type of problem is also known as rare event estimation in the recent statistics literature.

# 3 | Traditional approach

The main purpose of this case study is to analysis our data (349 simulations) that were obtained by using the PFC 3D code. The aim is supposed to calibrate the empirical formula which was defined in [13]. The traditional approach is traditional way based on interpolation by taking advantage of MATLAB in order to estimate the empirical formulae proposed by (Calvetti et al., 2017)[13] with the aim of finding a fitted curve between the maximum impact forces. The empirical formula eq.4 is a second-degree polynomial, Polyfit tools in MATLAB play a significant role in fitting the curves between the data and finding the most accurate empirical formula. The input parameters of the traditional approach are described below:

Table 2: Input parameters

$b$ (m)	$\gamma_s$	$v(m/s)$	$\alpha$	$h(m)$	$n$
2.4	25.5	[6.7-120.55]	[60°-70°-80°-90°]	[1.5-3-4.5-6-7.5]	[0.4-0.42]

$b$ : The width of model

$\gamma_s$ : Unit weight of particles

$v$ : Impact velocity

$\alpha$ : The front inclination

$h$ : The height of the barrier

$n$ : Initial porosity.

### 3.1. Maximum impact force action

The traditional approach implies that the data were obtained without calibration. Since the empirical formulae are normalised [13], the main aim of the traditional approach is to denormalise the eq.4 to facilitate the engineering perspective. In this procedure, the maximum impact force was used with the unit (MN), the Polyfit function in MATLAB would be the solution to our demand to find a fit between each of the two data points. However, degree 3 in our analysis marginally makes the fit better but the terms belonging to  $v^3$  do not have a physical meaning besides that from an engineering point of view, therefore the polynomial with degree 3 will not be considered in our analysis.

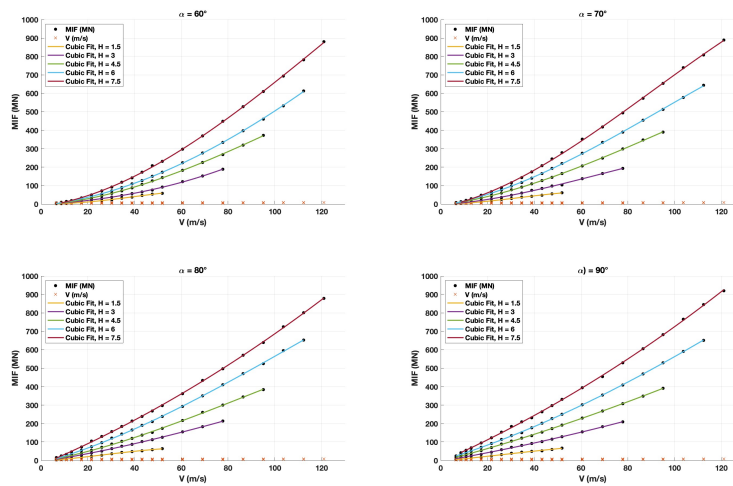


Figure 6: MIF versus Velocity for different conditions obtained by MATLAB Polynomial degrees 3

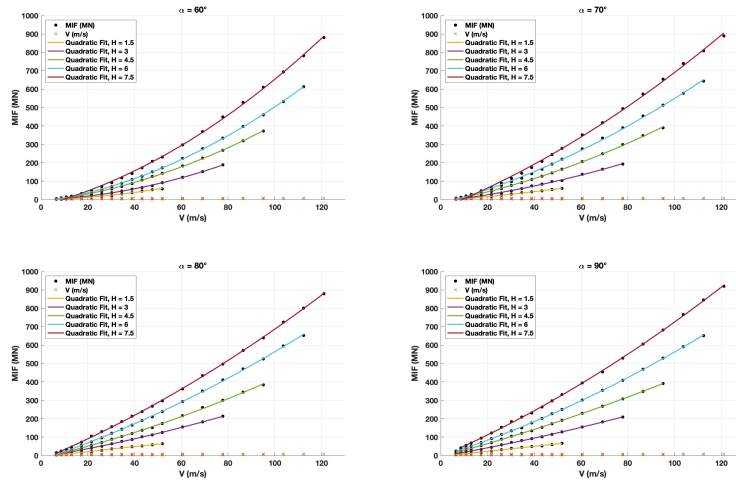


Figure 7: MIF versus Velocity for different conditions obtained by MATLAB Polynomial degrees 2

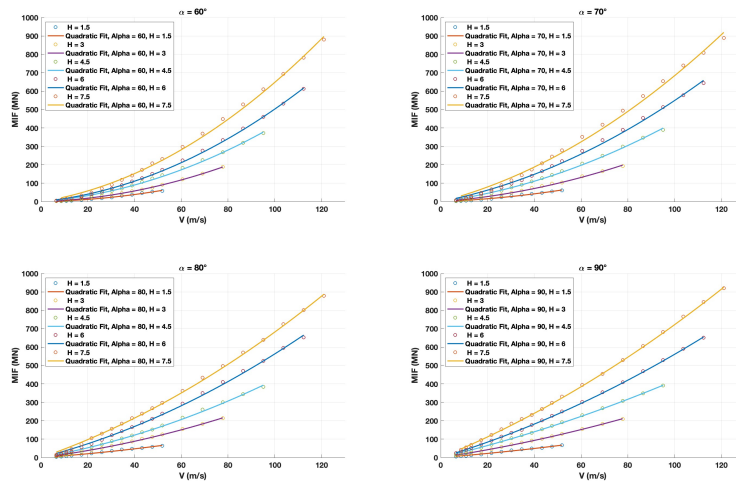


Figure 8: MIF versus Velocity for different conditions obtained by MATLAB Polynomial degrees 2 (Optimised)

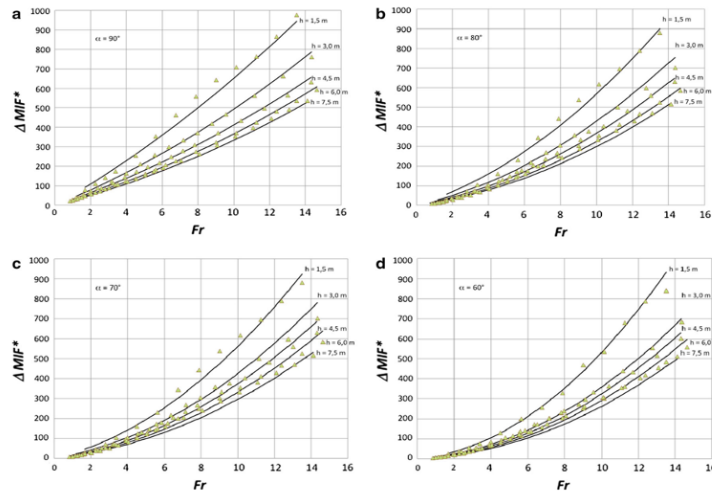


Figure 9:  $\Delta MIF^*$  versus  $Fr$ , numerical data and interpolation (eq.4) a=  $90^\circ$ , b=  $80^\circ$ , c= $70^\circ$ , d= $60^\circ$

Observing the difference between the fitted curves produced by MATLAB and the fitted curves obtained by interpolation in studied [13] significantly improved and denormalised. Elaborate on the code that was written, basically considering the input variables such as  $v$  (impact velocity),  $\alpha$  (Front inclination), and  $h$  (Flow height); the rest were constant inputs that did not consider for fitting curves and obtain the empirical formulae therefore such as  $b$  (Width of the model),  $\gamma_s$  (Unit weight of the particles) and  $n$  (initial porosity) and the output is maximum impact force ( $MIF$ ). In this approach, by implementing different types of fit functions in MATLAB, the single and integrated formula that will predict any condition is unattainable due to the complexity and uncertainty of the system. In order to find a reliable formula for the sake of complexity, the variables were separated to fit the curves.

Table 3: Empirical formula (Polynomial degrees 3)

$\alpha$	$h$ (m)	Formula
60°	1.5	$MIF = -0.00043335v^3 + 0.052911v^2 - 0.50559v + 3.4566$
	3	$MIF = 8.2618e^{-05}v^3 + 0.014606v^2 + 0.84592v - 3.868$
	4.5	$MIF = -0.00012972v^3 + 0.0448056v^2 + 0.86609v - 5.6497$
	6	$MIF = -6.1272e^{-05}v^3 + 0.043623v^2 + 1.3744v - 8.0311$
	7.5	$MIF = -0.00018165v^3 + 0.069451v^2 + 1.5978v - 12.7659$
70°	1.5	$MIF = -0.00043951v^3 + 0.044323v^2 + 0.043651v - 0.17232$
	3	$MIF = -0.00017229v^3 + 0.035779v^2 + 0.7901v - 3.9262$
	4.5	$MIF = -0.00012714v^3 + 0.038622v^2 + 1.6747v - 7.4228$
	6	$MIF = -0.00019196v^3 + 0.054849v^2 + 2.046v - 9.2492$
	7.5	$MIF = -0.00027551v^3 + 0.074728v^2 + 2.4543v - 16.3285$
80°	1.5	$MIF = -0.00031404v^3 + 0.024989v^2 + 0.83073v - 3.6082$
	3	$MIF = -3.4753e^{-05}v^3 + 0.013962v^2 + 1.9555v - 7.4873$
	4.5	$MIF = -0.00011744v^3 + 0.031293v^2 + 2.2174v - 6.9034$
	6	$MIF = -9.6005e^{-05}v^3 + 0.032905v^2 + 3.4572v - 14.1802$
	7.5	$MIF = 1.6052e^{-06}v^3 + 0.017317v^2 + 5.3486v - 22.9546$
90°	1.5	$MIF = -0.00011994v^3 + 0.010156v^2 + 1.1251v - 3.1267$
	3	$MIF = -3.6055e^{-06}v^3 + 0.0076409v^2 + 2.1854v - 4.6978$
	4.5	$MIF = -1.5661e^{-05}v^3 + 0.01109v^2 + 3.2543v - 4.9623$
	6	$MIF = -3.1122e^{-05}v^3 + 0.021242v^2 + 3.833v - 1.6055$
	7.5	$MIF = 8.7092e^{-06}v^3 + 0.016363v^2 + 5.5976v - 6.6287$

Table 4: Empirical formula (Polynomial degrees 2)

$\alpha$	$h$ (m)	Formula
60°	1.5	$MIF = 0.01515v^2 + 0.43189v - 2.535$
	3	$MIF = 0.024838v^2 + 0.4989v - 1.0732$
	4.5	$MIF = 0.025716v^2 + 1.6216v - 12.5374$
	6	$MIF = 0.033129v^2 + 1.8536v - 12.9517$
	7.5	$MIF = 0.035389v^2 + 3.3304v - 33.5664$
70°	1.5	$MIF = 0.0060233v^2 + 0.99447v - 6.2492$
	3	$MIF = 0.014442v^2 + 1.5137v - 9.7543$
	4.5	$MIF = 0.019914v^2 + 2.4152v - 14.1733$
	6	$MIF = 0.021972v^2 + 3.5472v - 24.6645$
	7.5	$MIF = 0.023067v^2 + 5.0821v - 47.8764$
80°	1.5	$MIF = -0.0023766v^2 + 1.5101v - 7.9502$
	3	$MIF = 0.0096576v^2 + 2.1015v - 8.6629$
	4.5	$MIF = 0.014012v^2 + 2.9015v - 13.1393$
	6	$MIF = 0.016462v^2 + 4.208v - 21.89$
	7.5	$MIF = 0.017612v^2 + 5.3342v - 22.7982$
90°	1.5	$MIF = -0.00029549v^2 + 1.3846v - 4.785$
	3	$MIF = 0.0071943v^2 + 2.2006v - 4.8198$
	4.5	$MIF = 0.008786v^2 + 3.3455v - 5.7938$
	6	$MIF = 0.015912v^2 + 4.0763v - 4.1048$
	7.5	$MIF = 0.017996v^2 + 5.5145v - 5.6314$

Table 5: MIF calculated by PFC 3D optimised empirical formulae

$\alpha$	$h$ (m)	Formula
60°	1.5	$MIF = 0.01841v^2 + 0.2254v$
	3	$MIF = 0.02575v^2 + 0.4146v$
	4.5	$MIF = 0.03116v^2 + 1.008v$
	6	$MIF = 0.03754v^2 + 1.272v$
	7.5	$MIF = 0.04457v^2 + 2.019v$
70°	1.5	$MIF = 0.01382v^2 + 0.4999v$
	3	$MIF = 0.02035v^2 + 0.9659v$
	4.5	$MIF = 0.02601v^2 + 1.728v$
	6	$MIF = 0.02983v^2 + 2.51v$
	7.5	$MIF = 0.03583v^2 + 3.26v$
80°	1.5	$MIF = 0.007505v^2 + 0.8835v$
	3	$MIF = 0.01493v^2 + 1.612v$
	4.5	$MIF = 0.0197v^2 + 2.261v$
	6	$MIF = 0.0235v^2 + 3.279v$
	7.5	$MIF = 0.02428v^2 + 4.39v$
90°	1.5	$MIF = 0.009461v^2 + 0.8589v$
	3	$MIF = 0.005713v^2 + 1.004v$
	4.5	$MIF = 0.01155v^2 + 3.035v$
	6	$MIF = 0.01771v^2 + 3.838v$
	7.5	$MIF = 0.02019v^2 + 5.201v$

By further observation of Table.4, it becomes apparent that during the initial step of the simulation, when the velocity is zero, the constant value of the formula tends to be a negative value which is irrelevant; therefore, by optimization, the constant value is eliminated in Table.5. The optimised quadratic functions can predict a reliable Maximum impact force respected to the normalised function in the article [13]. These MIF formulae with respect to normalised ones can be easily calculated the  $MIF$  with the unit of Mega Newton by putting the velocity with the unit m/s that can be predicted. Moreover, taking a look at Figure 8 and comparing it with Figure 9 clearly shows us that the new optimised second order polynomial formulae Table 5 work better.

## Correlation of coefficient versus $\alpha$ and $h$ for the optimised *MIF* empirical formula 2D representation

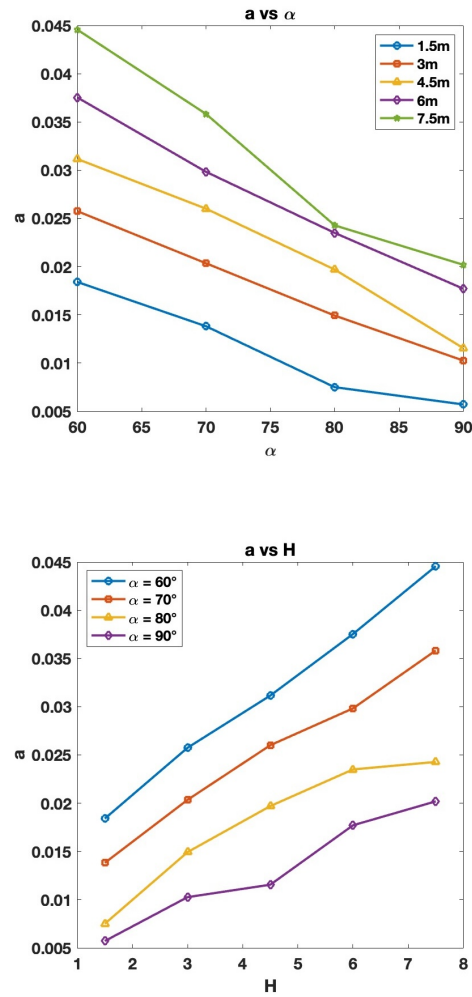


Figure 10: Comparison of the coefficient "a" for  $v^2$  term in the optimised empirical formulae with degree 2 between  $\alpha$  and  $h$

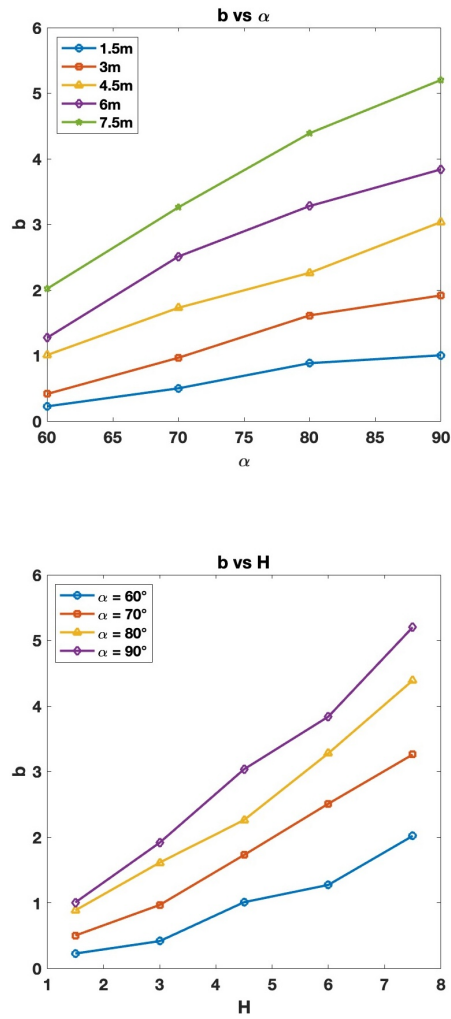


Figure 11: Comparison of the coefficient "b" for  $v$  term in the optimised empirical formulae with degree 2 between  $\alpha$  and  $h$

## Correlation of coefficient versus $\alpha$ and $h$ for the optimised *MIF* empirical formula 3D representation

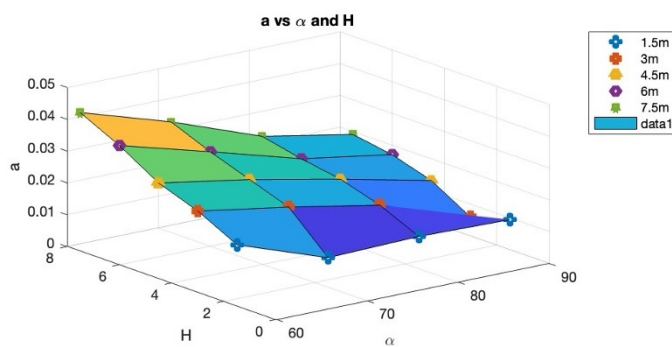


Figure 12: Comparison of the coefficient "a" for  $v^2$  term in the optimised empirical formulae with degree 2 between  $\alpha$  and  $h$  in 3D

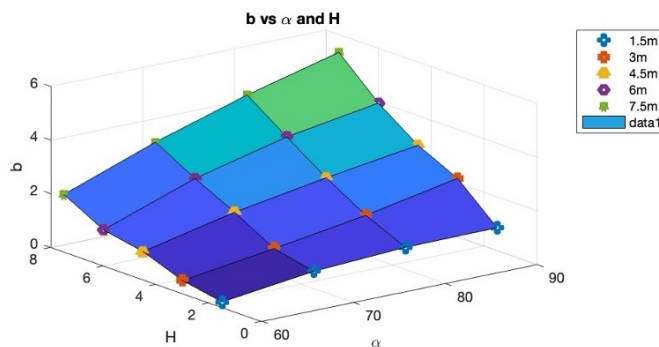


Figure 13: Comparison of the coefficient "b" for  $v$  term in the optimised empirical formulae with degree 2 between  $\alpha$  and  $h$  in 3D

## 3.2. Dynamic contribution to the Impact force

Consideration of passive thrust in the workflow had an insignificant influence on the  $\Delta_{MIF}$  empirical formulae. observation of Table 5 and 6 illustrate that the influence of passive thrust is negligible.

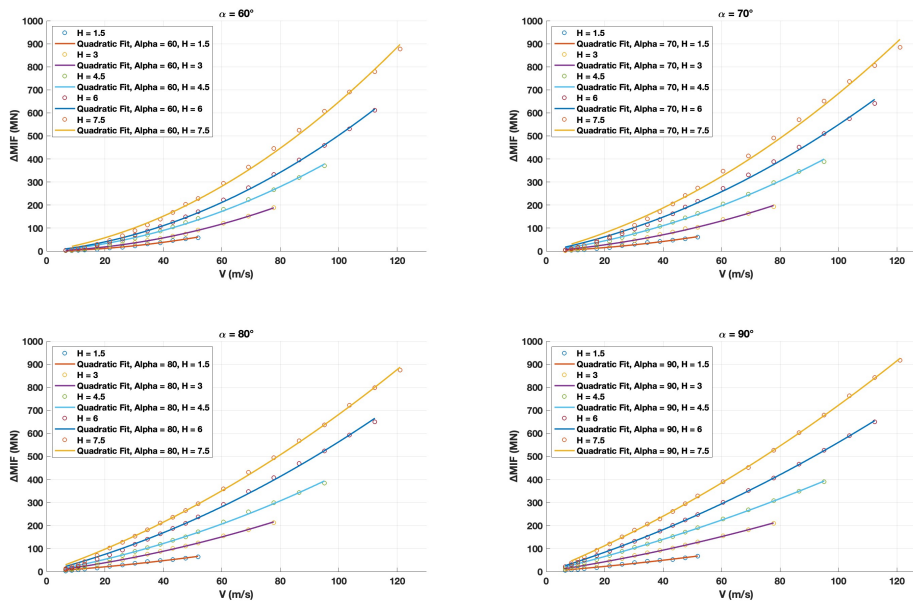


Figure 14:  $\Delta_{MIF}$  versus Velocity for different conditions obtained by MATLAB Polynomial degrees 2 (Optimised)

Table 6:  $\Delta_{MIF}$  versus Velocity for different conditions obtained by MATLAB Polynomial degrees 2 (Optimised)

$\alpha$	h (m)	Formula
60°	1.5	$\Delta_{MIF} = 0.01841v^2 + 0.2254v$
	3	$\Delta_{MIF} = 0.02575v^2 + 0.4146v$
	4.5	$\Delta_{MIF} = 0.03116v^2 + 1.008v$
	6	$\Delta_{MIF} = 0.03754v^2 + 1.272v$
	7.5	$\Delta_{MIF} = 0.04457v^2 + 2.019v$
70°	1.5	$\Delta_{MIF} = 0.01382v^2 + 0.4999v$
	3	$\Delta_{MIF} = 0.02035v^2 + 0.9659v$
	4.5	$\Delta_{MIF} = 0.02601v^2 + 1.728v$
	6	$\Delta_{MIF} = 0.02983v^2 + 2.51v$
	7.5	$\Delta_{MIF} = 0.03583v^2 + 3.26v$
80°	1.5	$\Delta_{MIF} = 0.007505v^2 + 0.8835v$
	3	$\Delta_{MIF} = 0.01493v^2 + 1.612v$
	4.5	$\Delta_{MIF} = 0.0197v^2 + 2.261v$
	6	$\Delta_{MIF} = 0.0235v^2 + 3.279v$
	7.5	$\Delta_{MIF} = 0.02428v^2 + 4.39v$
90°	1.5	$\Delta_{MIF} = 0.005713v^2 + 1.004v$
	3	$\Delta_{MIF} = 0.01026v^2 + 1.916v$
	4.5	$\Delta_{MIF} = 0.01155v^2 + 3.035v$
	6	$\Delta_{MIF} = 0.01771v^2 + 3.838v$
	7.5	$\Delta_{MIF} = 0.02019v^2 + 5.201v$

Correlation of coefficient versus  $\alpha$  and  $h$  for the optimised  $\Delta_{MIF}$  empirical formula 2D representation

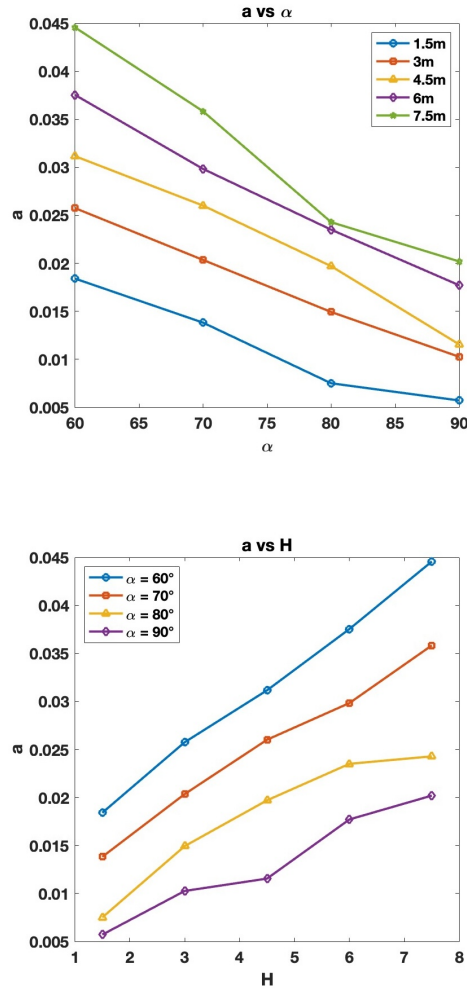


Figure 15: Comparison of the coefficient "a" for term  $v^2$  in the  $\Delta_{MIF}$  empirical formulae with degree 2 (Optimised) between  $\alpha$  and H

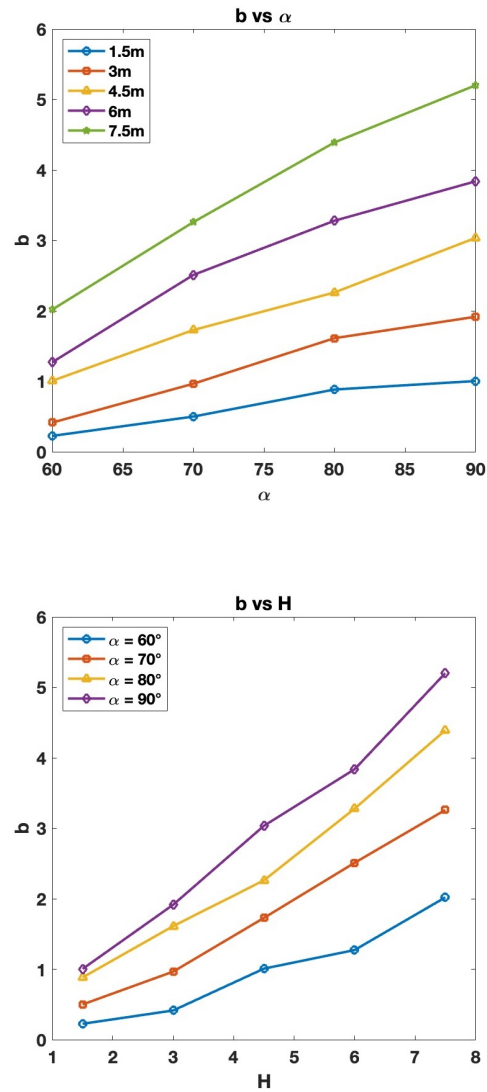


Figure 16: Comparison of the coefficient "b" for term  $v$  in the  $\Delta_{MIF}$  empirical formulae with degree 2 (Optimised) between  $\alpha$  and H

Correlation of coefficient versus  $\alpha$  and  $h$  for the optimised  $\Delta_{MIF}$  empirical formula 3D representation

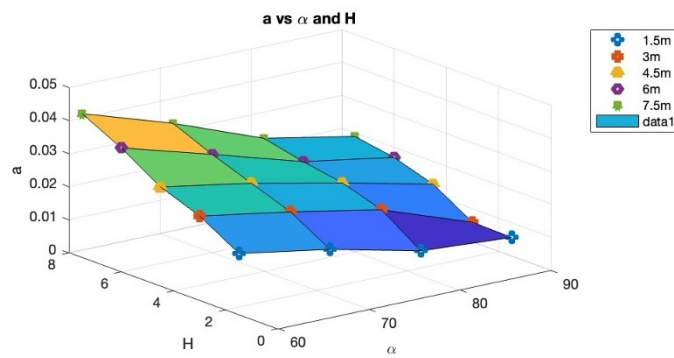


Figure 17: Comparison of the coefficient "a" for  $v^2$  term in the optimised  $\Delta_{MIF}$  empirical formulae with degree 2 between  $\alpha$  and  $h$  in 3D

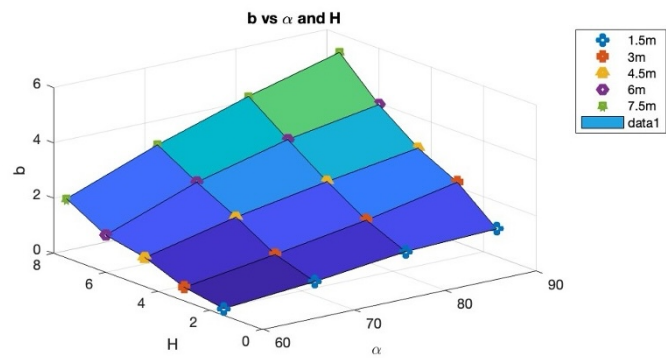


Figure 18: Comparison of the coefficient "b" for  $v$  term in the optimised  $\Delta_{MIF}$  empirical formulae with degree 2 between  $\alpha$  and  $h$  in 3D

### 3.3. Normalisation of Maximum Impact Force ( $\Delta_{MIF^*}$ )

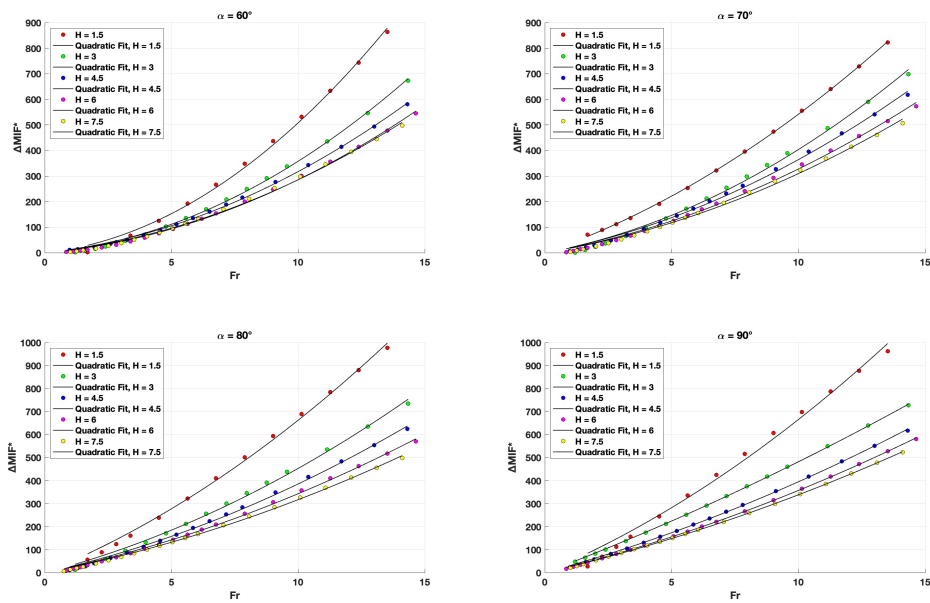


Figure 19:  $\Delta_{MIF^*}$  versus  $Fr$  for different conditions obtained by MATLAB Polynomial degrees 2 (Optimised)

Table 7: Normalised  $\Delta_{MIF^*}$  versus  $Fr$  (Optimised)

$\alpha$	h (m)	Formula
60°	1.5	$\Delta_{MIF^*} = 3.858Fr^2 + 12.32Fr$
	3	$\Delta_{MIF^*} = 2.698Fr^2 + 8.01Fr$
	4.5	$\Delta_{MIF^*} = 2.177Fr^2 + 10.6Fr$
	6	$\Delta_{MIF^*} = 1.967Fr^2 + 8.687Fr$
	7.5	$\Delta_{MIF^*} = 1.869Fr^2 + 9.868Fr$
70°	1.5	$\Delta_{MIF^*} = 2.898Fr^2 + 27.31Fr$
	3	$\Delta_{MIF^*} = 2.133Fr^2 + 18.66Fr$
	4.5	$\Delta_{MIF^*} = 1.817Fr^2 + 18.18Fr$
	6	$\Delta_{MIF^*} = 1.563Fr^2 + 17.15Fr$
	7.5	$\Delta_{MIF^*} = 1.502Fr^2 + 15.93Fr$
80°	1.5	$\Delta_{MIF^*} = 1.573Fr^2 + 48.28Fr$
	3	$\Delta_{MIF^*} = 1.565Fr^2 + 31.14Fr$
	4.5	$\Delta_{MIF^*} = 1.376Fr^2 + 23.78Fr$
	6	$\Delta_{MIF^*} = 1.232Fr^2 + 22.4Fr$
	7.5	$\Delta_{MIF^*} = 1.018Fr^2 + 21.45Fr$
90°	1.5	$\Delta_{MIF^*} = 1.198Fr^2 + 54.84Fr$
	3	$\Delta_{MIF^*} = 1.075Fr^2 + 37.02Fr$
	4.5	$\Delta_{MIF^*} = 0.8067Fr^2 + 31.91Fr$
	6	$\Delta_{MIF^*} = 0.9283Fr^2 + 26.22Fr$
	7.5	$\Delta_{MIF^*} = 0.8466Fr^2 + 25.42Fr$

### Correlation of coefficient versus $\alpha$ and $h$ for the optimised $\Delta_{MIF^*}$ empirical formula 2D representation

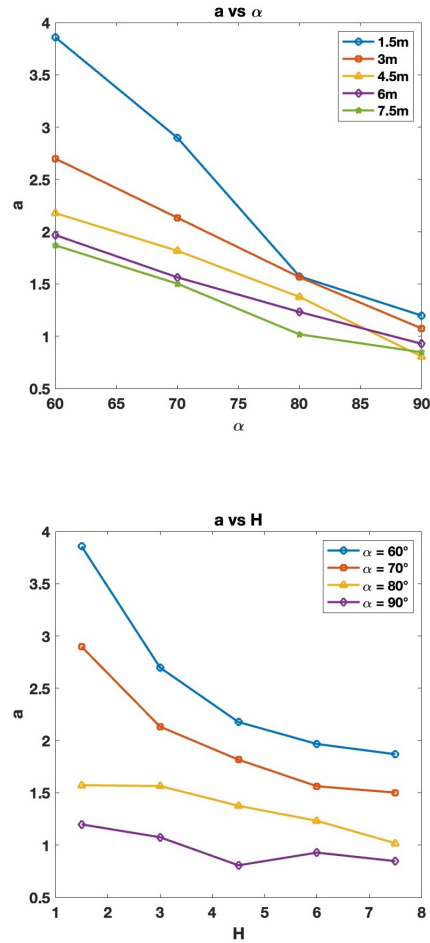


Figure 20: Comparison of the coefficient "a" for term  $Fr^2$  in the  $\Delta_{MIF^*}$  empirical formulae with degree 2 (Optimised) between  $\alpha$  and H

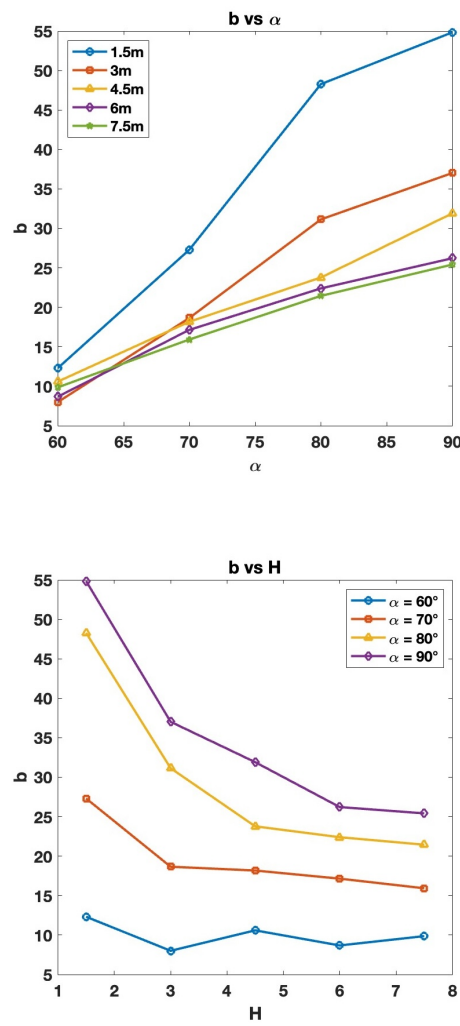


Figure 21: Comparison of the coefficient "b" for term  $Fr$  in the  $\Delta_{MIF}$ \* empirical formulae with degree 2 (Optimised) between  $\alpha$  and H

Correlation of coefficient versus  $\alpha$  and  $h$  for the optimised  $\Delta_{MIF^*}$  empirical formula 3D representation

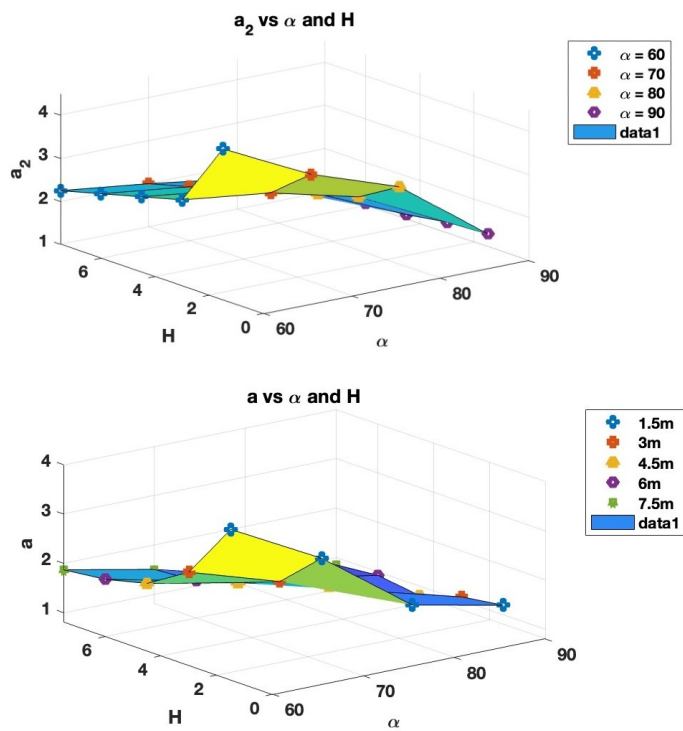


Figure 22: Comparison of the coefficients "a" and "a<sub>2</sub>" (from eq.4) for  $Fr^2$  term in the optimised  $\Delta_{MIF^*}$  empirical formulae with degree 2 between  $\alpha$  and  $h$  in 3D

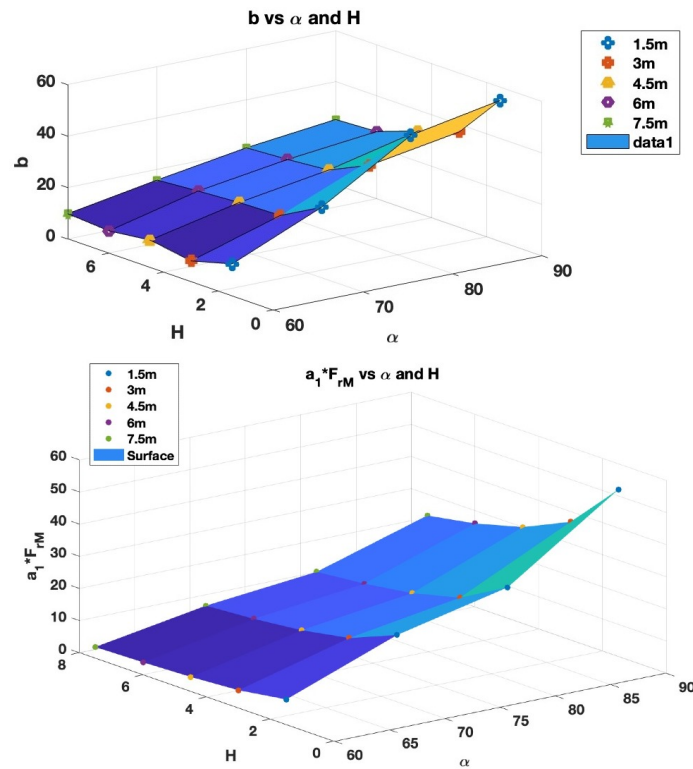


Figure 23: Comparison of the coefficient " $b$ " and " $a_1 * Fr_M$ " (from eq.4) for  $Fr$  term in the optimised  $\Delta_{MIF}$ \* empirical formulae with degree 2 between  $\alpha$  and  $h$  in 3D



# 4 | Meta-modelling approach

UQLAB [44] is a framework developed by ETH Zurich for uncertainty quantification, reliability analysis, sensitivity, and optimization of computational models. It provides a set of tools and functions to perform these analyses efficiently. The scripts were mainly written in MATLAB in the meta-modeling procedure, which UQLAB can do. The first step aims to decide which type of Meta will be reliable for the procedure. Since various Meta exist, the procedure can be started with Polynomial Chaos Expansion with different computational methods. By implementing PCE, it will be observed which Meta suits our workflow. In this step, 349 simulations are separated into train data (70%) and data validation (30%). A random function chose the training and validation data. One of the most crucial steps is knowing the effect constant values of inputs, such as the width  $b$ , porosity, and  $\gamma_s$  unit weight, and whether they can contribute to predicting Maximum impact force.

Table 8: Input parameters

$b$ (m)	$\gamma_s$	$v$ (m/s)	$\alpha$	$h$ (m)	$n$	$MIF(MN)$
2.4	25.5	[6.7 – 120.55]	[60° – 90°]	[1.5 – 7.5]	[0.4 – 0.42]	[1.7 – 920]

$b$ : The width of model

$\gamma_s$ : Unit weight of particles

$v$ : Impact velocity

$\alpha$ : The front inclination

$h$ : The height of the barrier

$n$ : Initial porosity

$MIF$ : Maximum Impact Force

## 4.1. Probabilistic Model

The module is used to define the probabilistic input model in uncertainty problems. It offers extensive possibilities to perform operations like drawing samples of random vectors or transforming samples of different random vectors (Iso-probabilistic transforms). The dependence structure between the components of random vectors is specified with the copula formalism. It also contains information about each available probability distribution that can be used in the current version of UQLab [44].

Table 9: Statistical approaches for probabilistic model

MC	Monte Carlo
LHS	Latin Hypercube
Sobol	Sobol series
Halton	Halton series

The existing simulations were distributed in Figure 24; to help the mode and optimise the campaign of numerical simulation, these statistical approaches from Table 9 depend on the user, which, in this case, assigns all the statistical approaches to observe the sample distribution to give an overview of different approaches. These distributions of data were done for the future study of this work. Unfortunately, this study is based on set of simulations they were not defined according to any probabilistic approaches 9 in particular simulations are represented 24 and compared with what should have been done according to such approaches such as Sobol series and Monte Carlo, Latin Hypercube, and Halton series distribution in Figures 25 26 27.

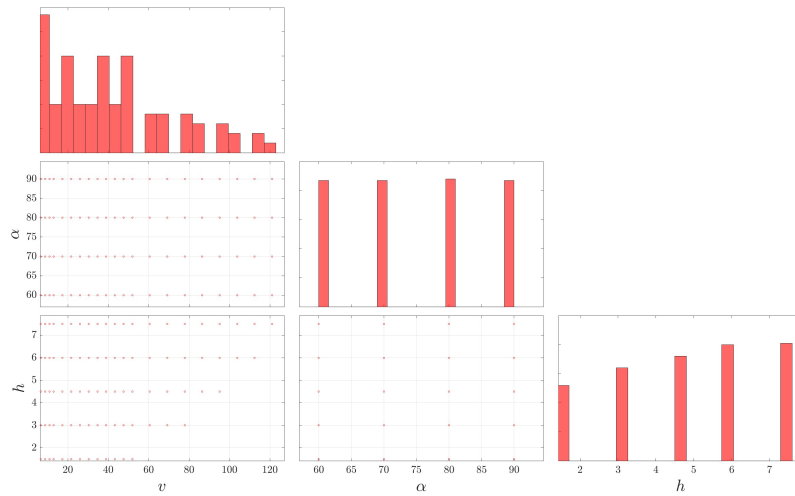


Figure 24: Scatter Density Plot data distribution using a defined script by author 244 (70%) input samples

Figure 25 is created by using the scatter density function, which was defined by the author based on some parameters containing: ‘eps’ a small constant used to control the separation between subplots in the Figure, ‘tol’ a tolerance parameter used in setting the x-axis and y-axis limits for histograms and scatter plots the usage of ‘tol’, multiplied by the sign of minimum and maximum values of each variable to determine the axis limits.  $x_{min}$  the minimum x-axis value for the entire Figure on the other word it defines the starting point for the x-axis, and  $x_{max}$  conversely defines the ending point of the x-axis, respectively the  $y_{min}$  and  $y_{max}$  were defined to do the action as described for the y-axis. ‘d’ is the dimensionality of the sample the other words, the number of variables determines the size of the subplot grid.

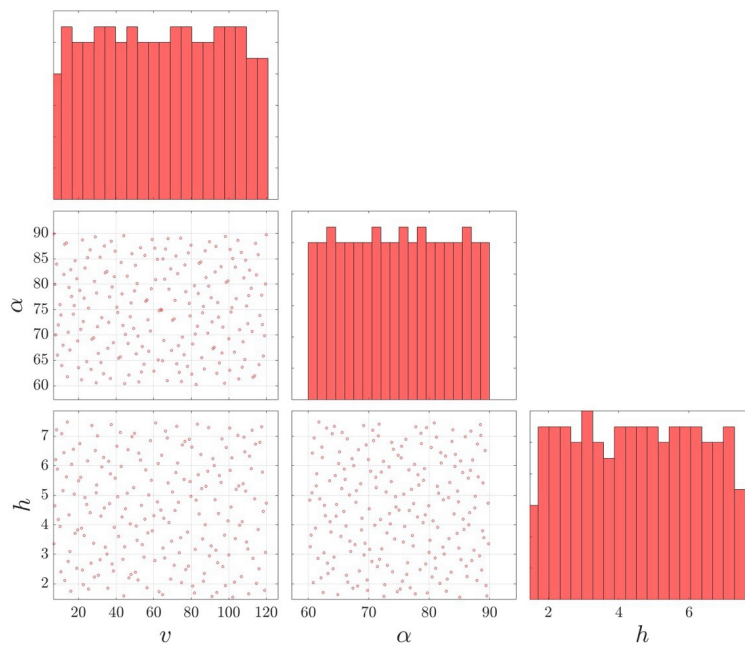


Figure 25: Scatter Density Plot based on Sobol series distribution using a defined script by author 244 (70%) input samples

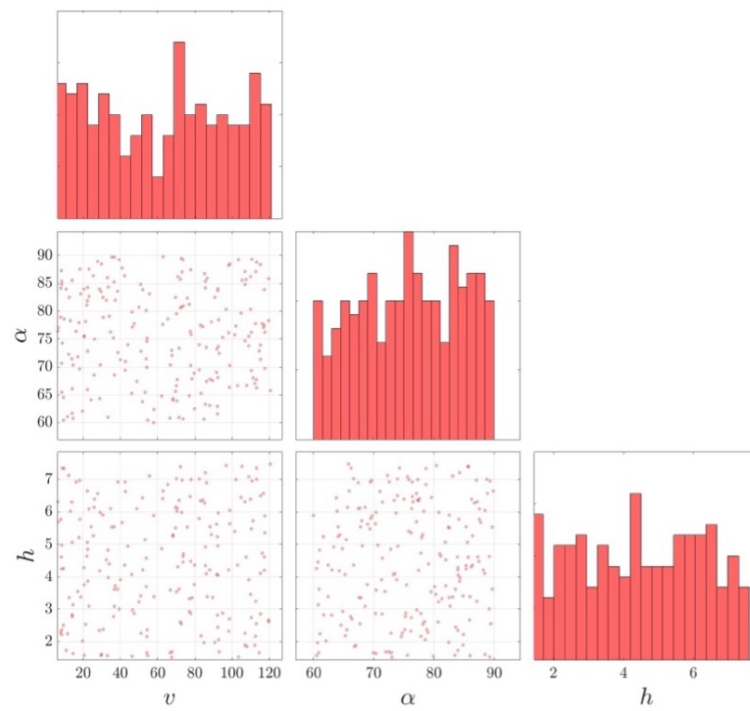


Figure 26: Scatter Density Plot based on Monte Carlo distribution using a defined script by author 244 (70%) input samples

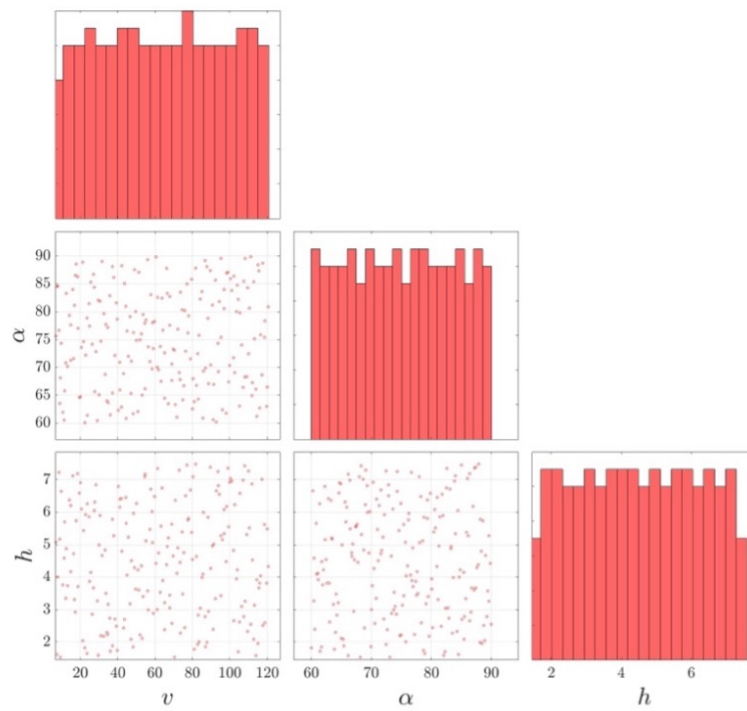


Figure 27: Scatter Density Plot based on Latin Hypercube distribution using a defined script by author 244 (70%) input samples

## 4.2. General overview of Polynomial Chaos Expansion with different computational methods:

Observation of Figure 28 and Figure 29 elaborate the accuracy of the predicted MIF based on different computational methods, and considering the quadrature method, we conclude that this method did not work at all; we are supposed to observe the computational errors that the script renders in Table 10.

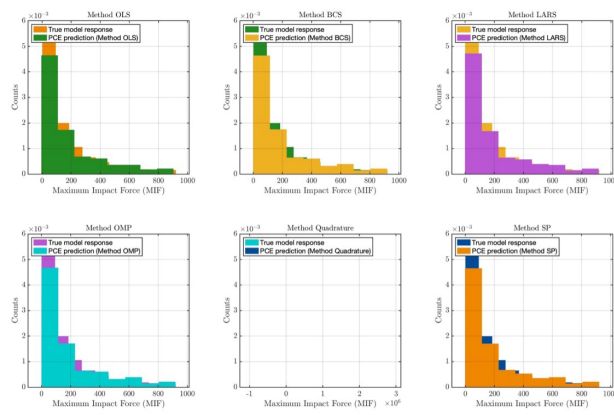


Figure 28: PCE Histogram for different computational methods, comparison between MIF and predicted MIF

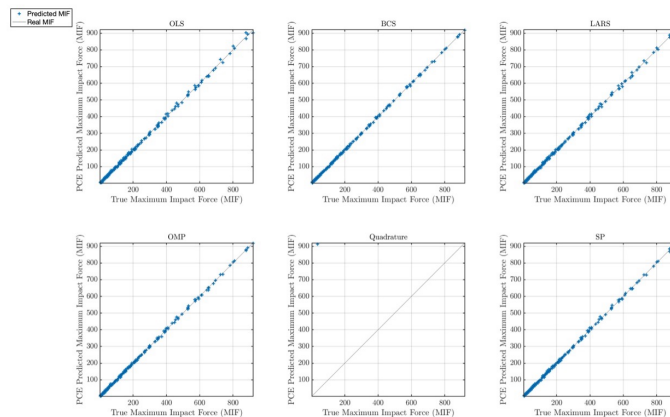


Figure 29: Distribution of predicted MIF around True MIF

The Table 10 illustrates the errors and statistical information related to a different types of meta-models and among these data, LOO is the important one, which is described below:

Table 10: Statistical information related to different methods and errors

Statistic	OLS	BCS	LARS	OMP	Quadrature	SP
Polynomial Degree	2	2	2	2	2	2
q-Norm	1.00	1.00	1.00	1.00	1.00	1.00
Full Basis Size	10	10	10	10	10	10
Sparse Basis Size	10	8	8	8	10	5
Full Model Evaluations	244	244	244	244	244	244
LOO Error Estimate	$1.526982 \times 10^{-3}$	$7.488826 \times 10^{-4}$	$9.004230 \times 10^{-4}$	$5.733753 \times 10^{-4}$	Quadrature Error	$6.147940 \times 10^{-4}$
Mean Value	241.6358	240.1570	249.1299	242.8475	7437.5502	241.2405
Standard Deviation	189.9764	189.8199	191.2235	191.5260	105353.2160	193.0657
Coefficient of Variation	78.621%	79.040%	76.757%	78.867%	1416.504%	80.030%
RMSE for Valid Data	$2.5305 \times 10^2$	$2.5299 \times 10^2$	$2.5290 \times 10^2$	$2.5323 \times 10^2$	$4.0302 \times 10^5$	$2.5292 \times 10^2$

### Definition of Leave-One-Out (LOO) Cross-Validation

Method: One data point is left out at a time, and the model is trained on the remaining data to predict the left-out point. This process is repeated for each data point.

The formula for LOO Cross-Validation Error ( $\varepsilon_{\text{LOO}}$ ):

$$\varepsilon_{\text{LOO}} = \frac{1}{N} \sum_{i=1}^N (y_i - \hat{y}_i)^2$$

- Where  $N$  is the total number of data points.
- $\varepsilon_{\text{LOO}}$ : represents the LOO Cross-Validation Error.
- $y_i$ : is the true observed value of the target variable for the  $i$ th data point.
- $\hat{y}_i$ : is the predicted value of the target variable for the  $i$ th data point obtained by the model trained on the remaining data points.
- The summation  $\sum_{i=1}^N$  is taken over all data points in the dataset.
- $(y_i - \hat{y}_i)^2$  represents the squared difference between the true and predicted values for each data point.

### **Benefits**

- Provides an unbiased estimate of the true error of a model.
- Valuable for model selection and comparison.

### **Drawbacks**

- Computationally expensive, especially for large datasets.
- Alternative methods, such as holdout cross-validation, may be preferred in some cases.

### 4.2.1. Sensitivity Analysis Sobol' Indices

Implementation of global sensitivity analysis Sobol's indices can be used to calculate first-order, second-order, and higher-order effects. First-order effects are the effects of an input parameter on the output without considering the effect of other input parameters. Total order effects are the effects of an input parameter on the output, considering the effects of more than one other input parameter. Sensitivity analysis can be calculated using a variety of methods, such as Monte Carlo methods; however, this method can be computationally expensive. In our analysis, the Polynomial chaos expansion method was implemented to calculate Sobol's indices. In order to express the reasoning behind discarding constant variables regarding the inputs, Sobol's indices are conducted in Figure 30. The range of Sobol indices are between 0 and 1, and the sum of Sobol indices are equal to 1.

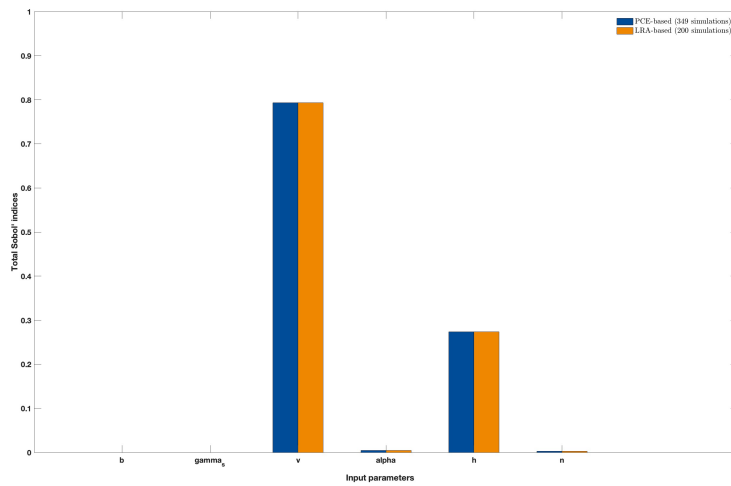


Figure 30: Sobol' indices diagram

Table 11: . Total Sobol' indices for all the inputs

Parameter	$b$	$\gamma_s$	$v$	$\alpha$	$h$	$n$
Value	0.000000	0.000000	0.793491	0.004425	0.199659	0.002425

However, the sensitivity analysis in Figure 30 might not be correct in the sense that by observation of Figure 12 13, it is obvious the effect of front inclination is not almost negligible, and these values were obtained due to incorrect implementation of sensitivity analysis which constant parameters lead to misinterpreting the effectiveness of inputs variables, therefore, sensitivity analysis was repeated by disregarding constant variables in order to obtain a reasonable results Figure 32.

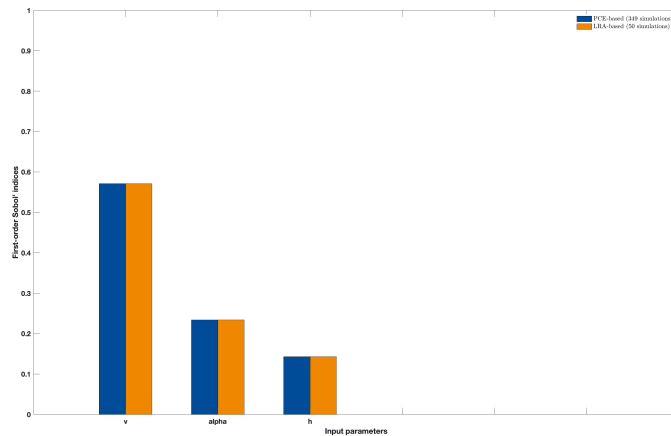


Figure 31: First order Sobol' indices diagram for input variable parameters

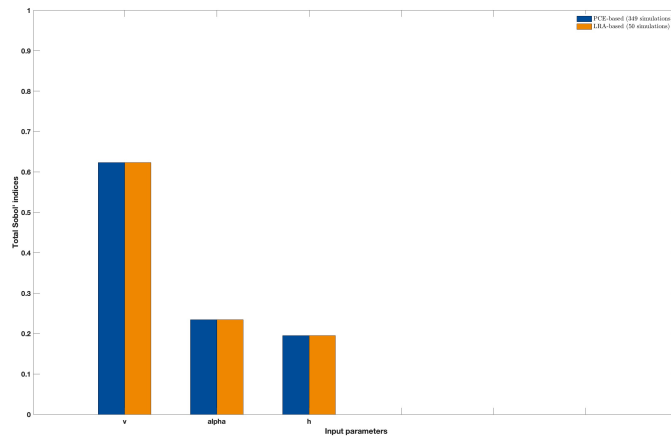


Figure 32: Total order Sobol' indices diagram for input variable parameters

Table 12: . Total Sobol' indices for all the inputs

Parameter	$v$	$\alpha$	$h$
Value	0.61206	0.214546	0.173394

In table 12, the effectivity of  $\alpha$  increased with respect to the previous analysis. It is worth mentioning that these data still are not reliable and rich enough to be taken into account.

### 4.2.2. Meta-model based on Bayesian Compressive Sensing (BCS)

By analysing the Table 10. Attentively, Bayesian Compressive Sensing (BCS) and Least Angle Regression (LARS) can be chosen for the rest of the procedure of meta-modelling. In this case, the author considered constructing a meta-model by using Bayesian Compressive Sensing (BCS) "Appendix A".

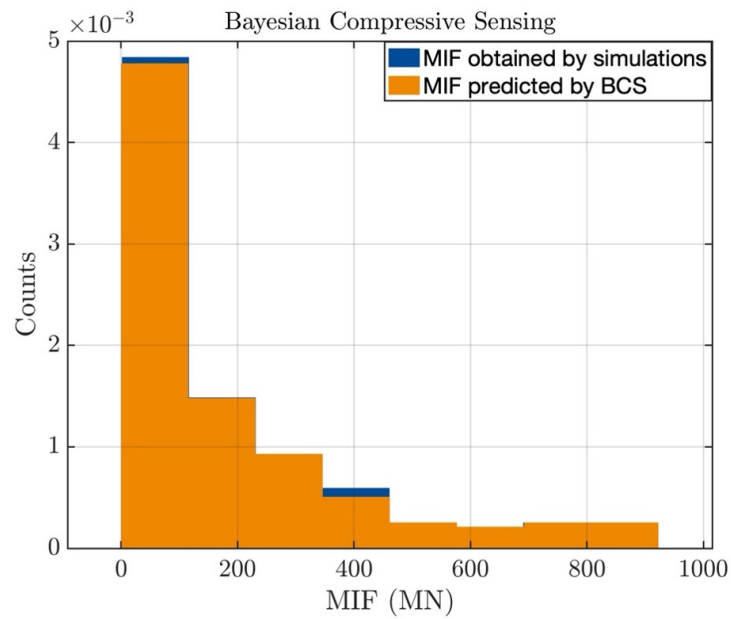


Figure 33: PCE Histogram for Bayesian, compressive between MIF and predicted MIF

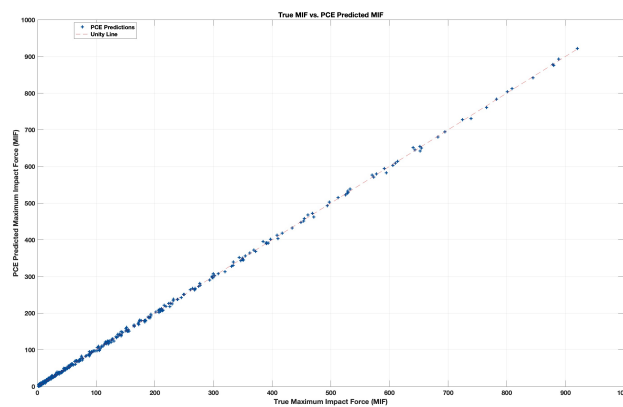


Figure 34: MIF predicted by meta-model versus MIF (PFC3D)

Once the meta-model has been built, the meta has the capability to predict the maximum impact force for any value which exists within the range defined for each input parameter Figure 35. Since the meta was constructed by polynomial chaos expansion, in Figure 36 the machine trained with new input data for different heights "Appendix B", and in Figure 37 trained for new front inclination.

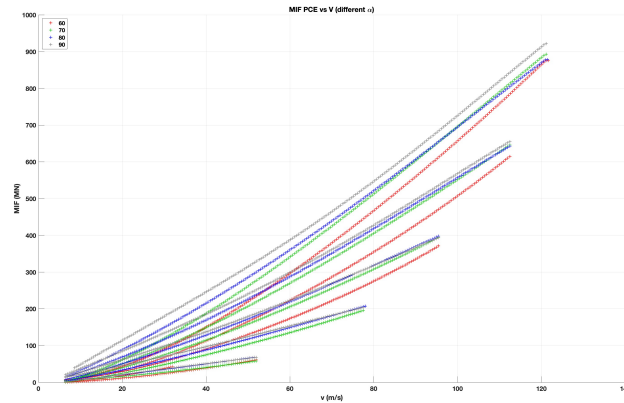


Figure 35: MIF predicted by meta-model versus velocity

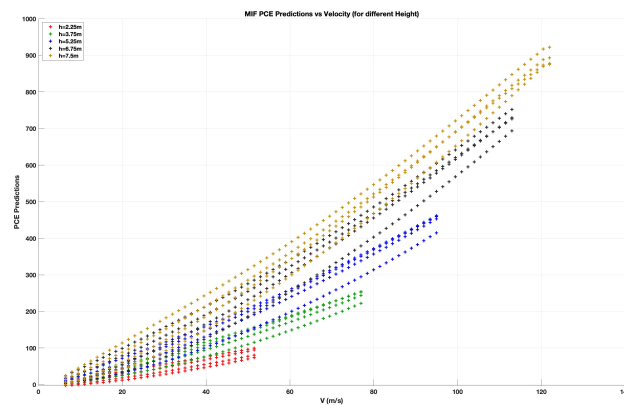


Figure 36: MIF predicted by meta-model versus velocity for the new heights

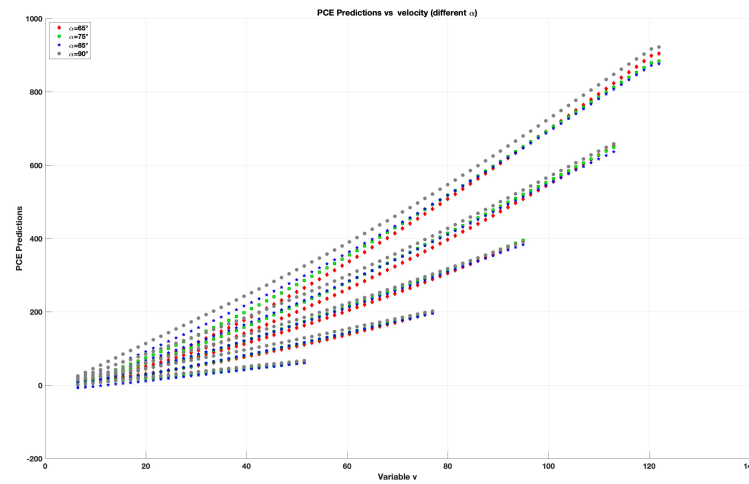


Figure 37: MIF predicted by meta-model versus velocity for the new inclination

The output of the meta-model is replaced by the output of the simulation, which was obtained by PFC 3D. The numerical approach in case study 1 was analysed with the advantage of using a meta-model. Using the Polyfit function in MATLAB was implemented to repeat the analysis in case study 1 in order to do modifications and calibrate the empirical formula [13] proposed by Calvetti.

### Interpretation of the results of the Meta-model

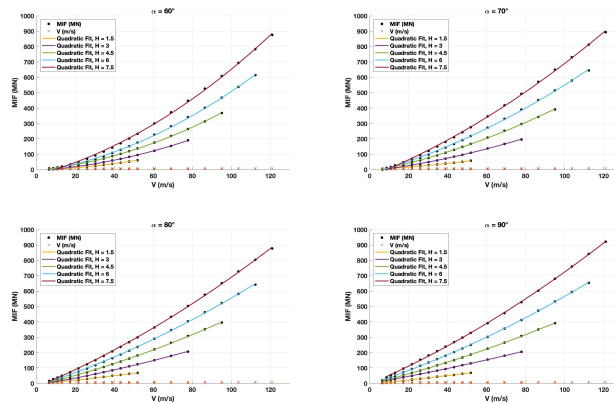


Figure 38: MIF versus Velocity for different conditions obtained by MATLAB Polynomial degrees 2

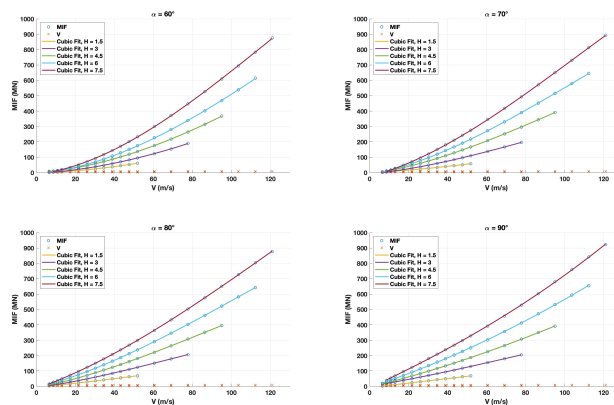


Figure 39: MIF versus Velocity for different conditions obtained by MATLAB Polynomial degrees 3

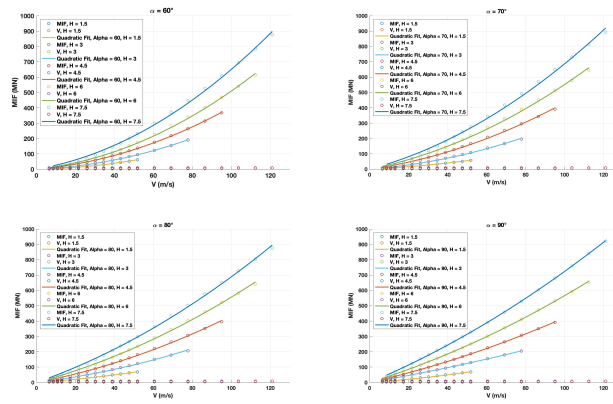


Figure 40: MIF versus Velocity for different conditions obtained by MATLAB Polynomial degrees 2 (Optimised)

Table 12: *MIF* Empirical formula for meta-model output (Polynomial degrees 3)

$\alpha$	$h$ (m)	Formula
60°	1.5	$MIF = -4.28e - 05v^3 + 0.01807v^2 + 0.4109v - 3.332$
	3	$MIF = -2.832e - 05v^3 + 0.02532v^2 + 0.7004v - 5.356$
	4.5	$MIF = -7.438e - 05v^3 + 0.03912v^2 + 0.8175v - 0.6032$
	6	$MIF = -0.0001262v^3 + 0.05443v^2 + 0.968v - 5.679$
	7.5	$MIF = -0.0001995v^3 + 0.07247v^2 + 1.455v - 11.12$
70°	1.5	$MIF = -0.0001096v^3 + 0.01908v^2 + 0.385v + 1.746$
	3	$MIF = -9.437e - 05v^3 + 0.02576v^2 + 1.201v - 8.59$
	4.5	$MIF = -0.0001182v^3 + 0.03625v^2 + 1.837v - 9.711$
	6	$MIF = -0.0001467v^3 + 0.04701v^2 + 2.432v - 14.61$
	7.5	$MIF = -0.0001786v^3 + 0.05674v^2 + 3.333v - 25.57$
80°	1.5	$MIF = -0.0001171v^3 + 0.01545v^2 + 0.8823v - 2.32$
	3	$MIF = -0.000101v^3 + 0.02156v^2 + 1.695v - 8.03$
	4.5	$MIF = -0.0001026v^3 + 0.02874v^2 + 2.454v - 9.268$
	6	$MIF = -0.0001078v^3 + 0.03496v^2 + 3.231v - 8.767$
	7.5	$MIF = -9.684e - 05v^3 + 0.03607v^2 + 4.439v - 14.23$
90°	1.5	$MIF = -6.517e - 05v^3 + 0.005805v^2 + 1.31v - 6.729$
	3	$MIF = -4.834e - 05v^3 + 0.01133v^2 + 2.038v + 0.5127$
	4.5	$MIF = -2.771e - 05v^3 + 0.01521v^2 + 2.972v - 3.746$
	6	$MIF = -9.61e - 06v^3 + 0.01689v^2 + 4.119v - 5.329$
	7.5	$MIF = 4.139e - 05v^3 + 0.009993v^2 + 5.916v - 10.05$

Table 13: *MIF* Empirical formula for meta-model output (Polynomial degrees 2)

$\alpha$	$h$ (m)	Formula
60°	1.5	$MIF = 0.01434v^2 + 0.5034v - 3.924$
	3	$MIF = 0.02182v^2 + 0.8194v - 6.314$
	4.5	$MIF = 0.02817v^2 + 1.251v - 4.553$
	6	$MIF = 0.03282v^2 + 1.955v - 15.81$
	7.5	$MIF = 0.03506v^2 + 3.358v - 33.97$
70°	1.5	$MIF = 0.009529v^2 + 0.6222v + 0.2304$
	3	$MIF = 0.01407v^2 + 1.598v - 11.78$
	4.5	$MIF = 0.01885v^2 + 2.526v - 15.99$
	6	$MIF = 0.02189v^2 + 3.579v - 26.39$
	7.5	$MIF = 0.02326v^2 + 5.036v - 46.01$
80°	1.5	$MIF = 0.005249v^2 + 1.136v - 3.939$
	3	$MIF = 0.009042v^2 + 2.12v - 11.45$
	4.5	$MIF = 0.01363v^2 + 3.052v - 14.72$
	6	$MIF = 0.01649v^2 + 4.074v - 17.43$
	7.5	$MIF = 0.01828v^2 + 5.307v - 23.67$
90°	1.5	$MIF = 0.0001262v^2 + 1.451v - 7.63$
	3	$MIF = 0.005347v^2 + 2.241v - 1.122$
	4.5	$MIF = 0.01113v^2 + 3.133v - 5.217$
	6	$MIF = 0.01524v^2 + 4.194v - 6.1$
	7.5	$MIF = 0.01775v^2 + 5.521v - 5.313$

Table 14: Optimised *MIF* Empirical formula for meta-model output (Polynomial degrees 2)

$\alpha$	$h$ (m)	Formula
60°	1.5	$MIF = 0.01914v^2 + 0.199v$
	3	$MIF = 0.02545v^2 + 0.4822v$
	4.5	$MIF = 0.02998v^2 + 1.046v$
	6	$MIF = 0.03747v^2 + 1.34v$
	7.5	$MIF = 0.04355v^2 + 2.145v$
70°	1.5	$MIF = 0.009247v^2 + 0.6401v$
	3	$MIF = 0.02086v^2 + 0.9687v$
	4.5	$MIF = 0.02522v^2 + 1.809v$
	6	$MIF = 0.02966v^2 + 2.554v$
	7.5	$MIF = 0.03476v^2 + 3.393v$
80°	1.5	$MIF = 0.01007v^2 + 0.83v$
	3	$MIF = 0.01563v^2 + 1.508v$
	4.5	$MIF = 0.01949v^2 + 2.391v$
	6	$MIF = 0.02162v^2 + 3.397v$
	7.5	$MIF = 0.02437v^2 + 4.446v$
90°	1.5	$MIF = 0.009461v^2 + 0.8589v$
	3	$MIF = 0.005993v^2 + 2.181v$
	4.5	$MIF = 0.01321v^2 + 2.899v$
	6	$MIF = 0.01704v^2 + 3.957v$
	7.5	$MIF = 0.01908v^2 + 5.331v$

## Correlation of coefficient versus $\alpha$ and $h$ for the optimised *MIF* empirical formula 2D representation

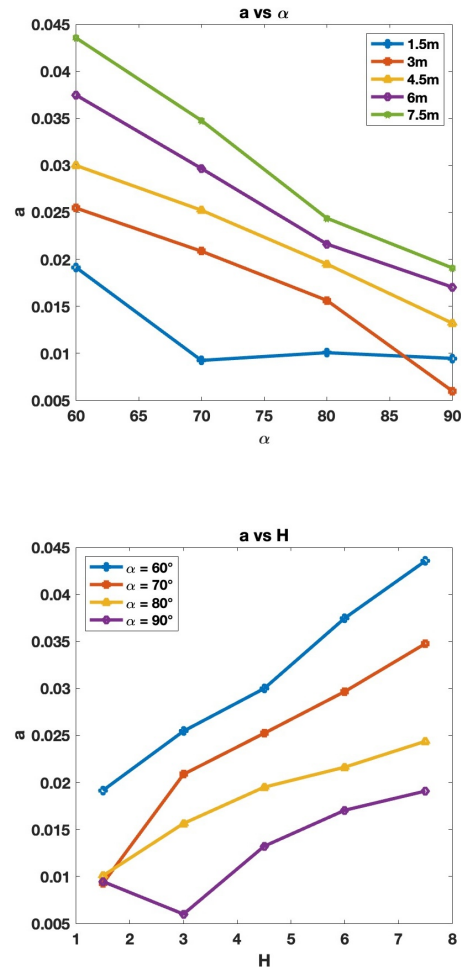


Figure 41: Comparison of the coefficient "a" for  $v^2$  term in the optimised empirical formulae with degree 2 between alpha and h

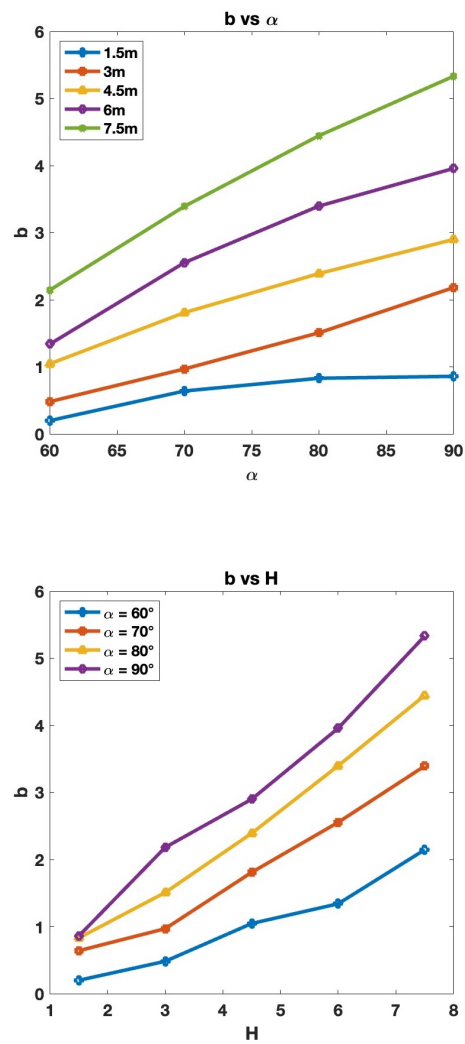


Figure 42: Comparison of the coefficient "b" for  $v$  term in the optimised empirical formulae with degree 2 between  $\alpha$  and  $h$

### Correlation of coefficient versus $\alpha$ and $h$ for the optimised *MIF* empirical formula predicted by meta.model 3D representation

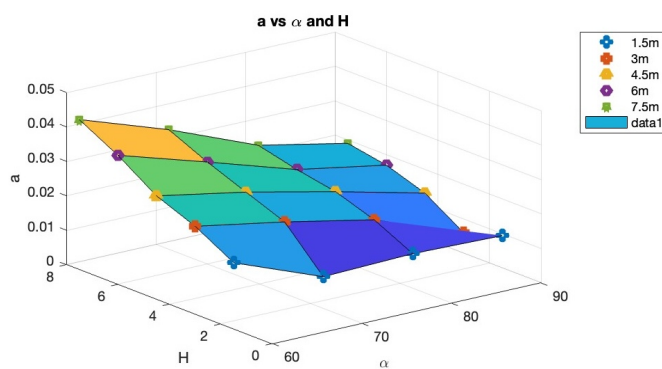


Figure 43: Comparison of the coefficient "a" for  $v^2$  term in the optimised *MIF* empirical formulae obtained by meta-model with degree 2 between  $\alpha$  and  $h$  in 3D

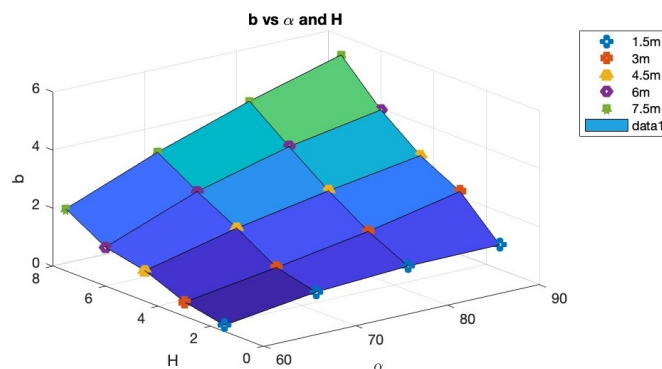


Figure 44: Comparison of the coefficient "b" for  $v$  term in the optimised *MIF* empirical formulae obtained by meta-model with degree 2 between  $\alpha$  and  $h$  in 3D

### 4.3. Dynamic contribution to the Impact force

Consideration of passive thrust in the workflow had an insignificant influence on the  $\Delta_{MIF}$  empirical formulae.

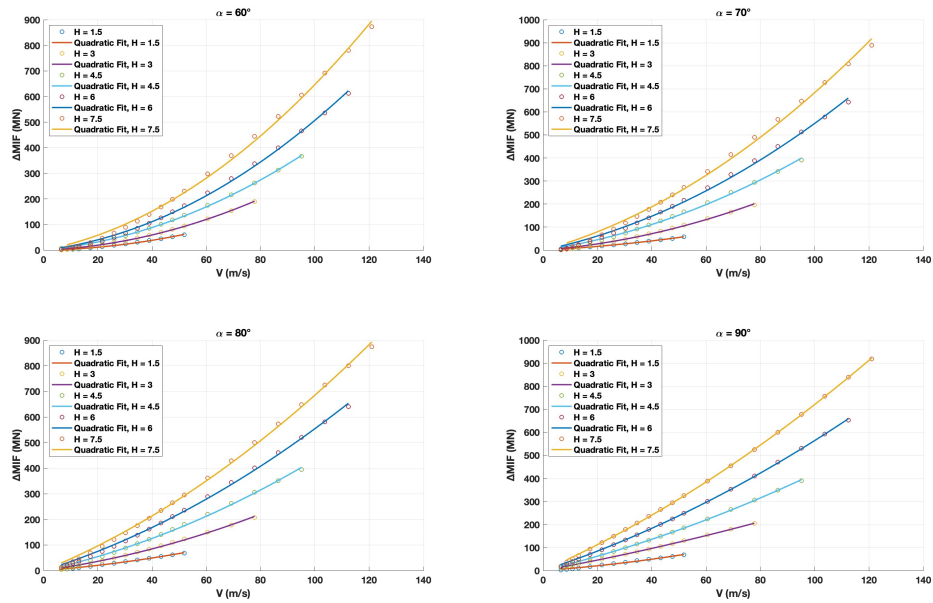


Figure 45:  $\Delta_{MIF}$  versus Velocity for different conditions obtained by MATLAB Polynomial degrees 2 (Optimised)

Table 15: Optimised *MIF* Empirical formula for meta-model output (Polynomial degrees 2)

$\alpha$	$h$ (m)	Formula
60°	1.5	$\Delta MIF = 0.0193v^2 + 0.1892v$
	3	$\Delta MIF = 0.02574v^2 + 0.4552v$
	4.5	$\Delta MIF = 0.03044v^2 + 0.9955v$
	6	$\Delta MIF = 0.03807v^2 + 1.262v$
	7.5	$\Delta MIF = 0.04434v^2 + 2.032v$
70°	1.5	$\Delta MIF = 0.009402v^2 + 0.6303v$
	3	$\Delta MIF = 0.02115v^2 + 0.9417v$
	4.5	$\Delta MIF = 0.02567v^2 + 1.758v$
	6	$\Delta MIF = 0.03025v^2 + 2.475v$
	7.5	$\Delta MIF = 0.03555v^2 + 3.281v$
80°	1.5	$\Delta MIF = 0.01022v^2 + 0.8202v$
	3	$\Delta MIF = 0.01592v^2 + 1.481v$
	4.5	$\Delta MIF = 0.01994v^2 + 2.34v$
	6	$\Delta MIF = 0.02221v^2 + 3.319v$
	7.5	$\Delta MIF = 0.02518v^2 + 4.331v$
90°	1.5	$\Delta MIF = 0.009616v^2 + 0.8491v$
	3	$\Delta MIF = 0.006284v^2 + 2.154v$
	4.5	$\Delta MIF = 0.01366v^2 + 2.848v$
	6	$\Delta MIF = 0.01763v^2 + 3.878v$
	7.5	$\Delta MIF = 0.01987v^2 + 5.218v$

## Correlation of coefficient versus $\alpha$ and $h$ for the optimised $\Delta_{MIF}$ empirical formula 2D representation

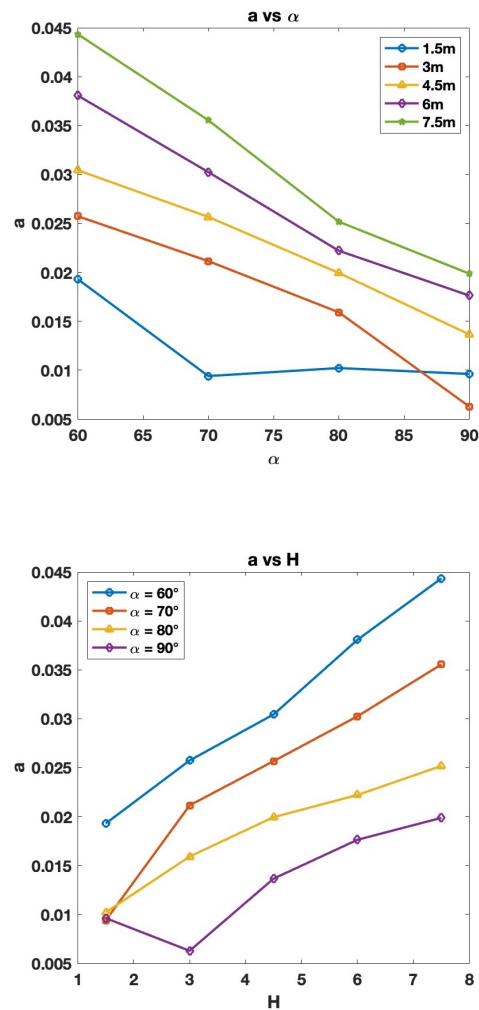


Figure 46: Comparison of the coefficient "a" for  $v^2$  term in the optimised  $\Delta_{MIF}$  empirical formulae with degree 2 between  $\alpha$  and  $h$  in 2D

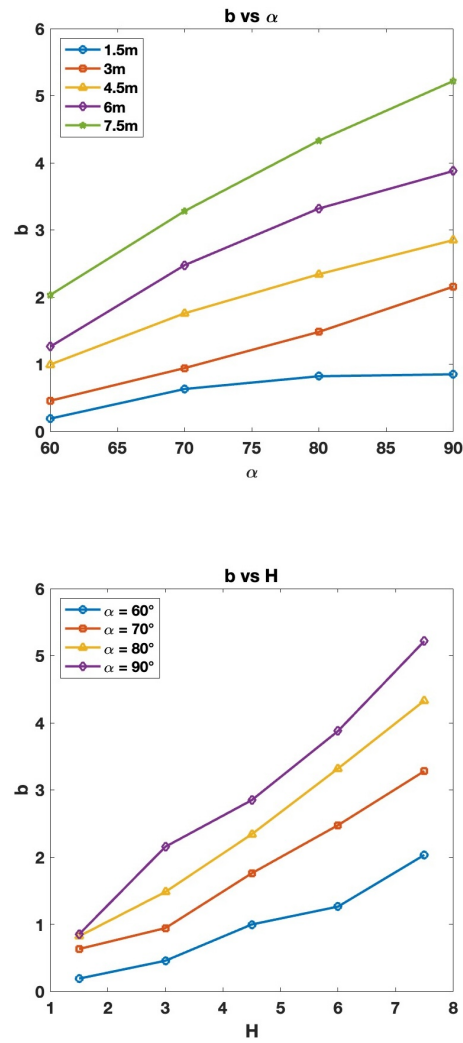


Figure 47: Comparison of the coefficient "b" for  $v$  term in the optimised  $\Delta_{MIF}$  empirical formulae with degree 2 between  $\alpha$  and  $h$  in 2D

Correlation of coefficient versus  $\alpha$  and  $h$  for the optimised  $\Delta_{MIF}$  empirical formula predicted by meta.model 3D representation

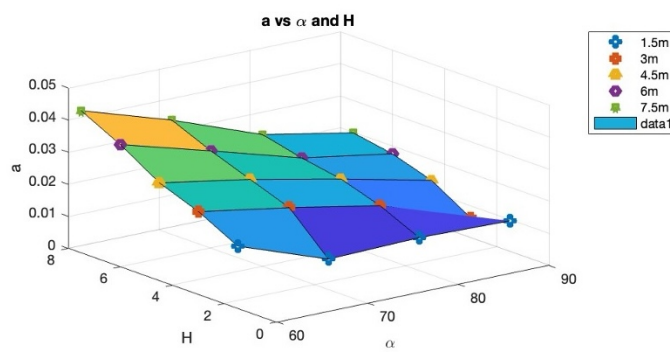


Figure 48: Comparison of the coefficient "a" for  $v^2$  term in the optimised  $\Delta_{MIF}$  empirical formulae with degree 2 between alpha and h

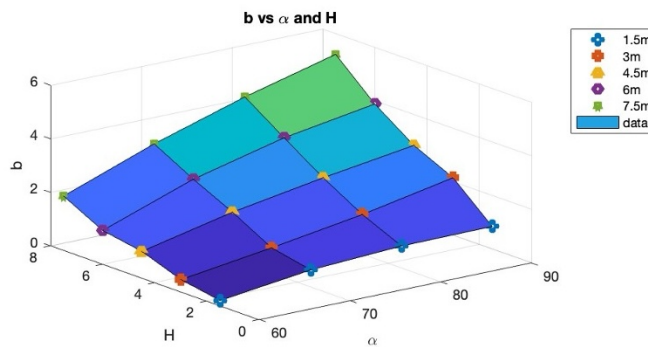


Figure 49: Comparison of the coefficient "b" for  $v$  term in the optimised  $\Delta_{MIF}$  empirical formulae with degree 2 between alpha and h

#### 4.4. Normalisation of Maximum Impact Force ( $\Delta_{MIF^*}$ ) obtained by meta-model

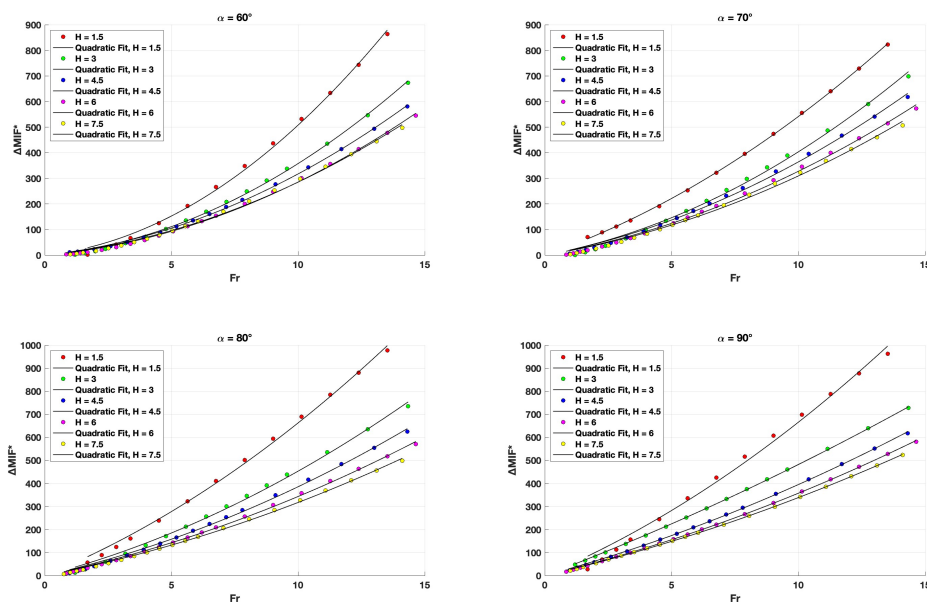


Figure 50:  $\Delta_{MIF^*}$  versus  $Fr$  for different conditions obtained by MATLAB Polynomial degrees 2 (Optimised) obtained by meta-model

Table 16: Normalised  $\Delta_{MIF^*}$  versus  $Fr$  (Optimised)

60°	1.5	$\Delta_{MIF^*} = 4.045Fr^2 + 10.34Fr$
	3	$\Delta_{MIF^*} = 2.698Fr^2 + 8.795Fr$
	4.5	$\Delta_{MIF^*} = 2.127Fr^2 + 10.47Fr$
	6	$\Delta_{MIF^*} = 1.995Fr^2 + 8.619Fr$
	7.5	$\Delta_{MIF^*} = 1.859Fr^2 + 9.934Fr$
70°	1.5	$\Delta_{MIF^*} = 1.971Fr^2 + 34.44Fr$
	3	$\Delta_{MIF^*} = 2.216Fr^2 + 18.19Fr$
	4.5	$\Delta_{MIF^*} = 1.794Fr^2 + 18.48Fr$
	6	$\Delta_{MIF^*} = 1.585Fr^2 + 16.91Fr$
	7.5	$\Delta_{MIF^*} = 1.491Fr^2 + 16.03Fr$
80°	1.5	$\Delta_{MIF^*} = 2.143Fr^2 + 44.82Fr$
	3	$\Delta_{MIF^*} = 1.669Fr^2 + 28.62Fr$
	4.5	$\Delta_{MIF^*} = 1.394Fr^2 + 24.61Fr$
	6	$\Delta_{MIF^*} = 1.164Fr^2 + 22.67Fr$
	7.5	$\Delta_{MIF^*} = 1.055Fr^2 + 21.17Fr$
90°	1.5	$\Delta_{MIF^*} = 2.016Fr^2 + 46.4Fr$
	3	$\Delta_{MIF^*} = 0.6586Fr^2 + 41.61Fr$
	4.5	$\Delta_{MIF^*} = 0.9544Fr^2 + 29.95Fr$
	6	$\Delta_{MIF^*} = 0.924Fr^2 + 26.49Fr$
	7.5	$\Delta_{MIF^*} = 0.8331Fr^2 + 25.5Fr$

### Correlation of coefficient versus $\alpha$ and $h$ for the optimised $\Delta_{MIF}^*$ empirical formula 2D representation

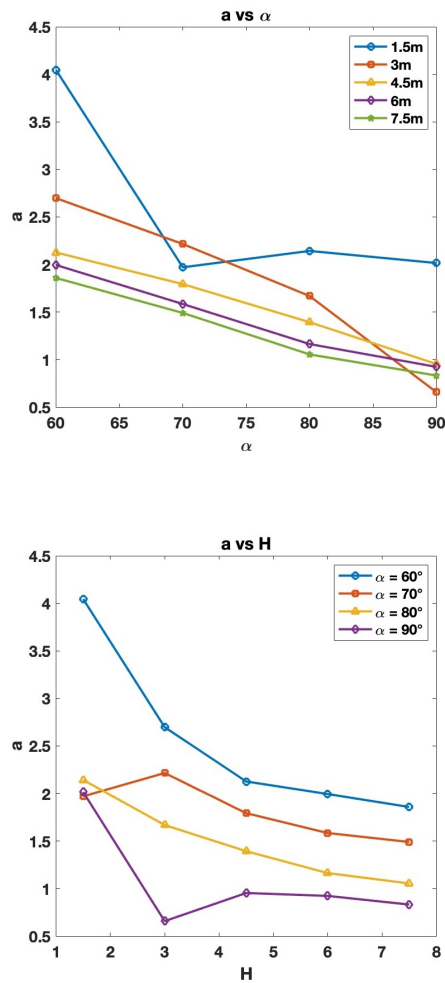


Figure 51: Comparison of the coefficient "a" for term  $Fr^2$  in the  $\Delta_{MIF}^*$  empirical formulae obtained by the Meta-model with degree 2 (Optimised) between  $\alpha$  and H

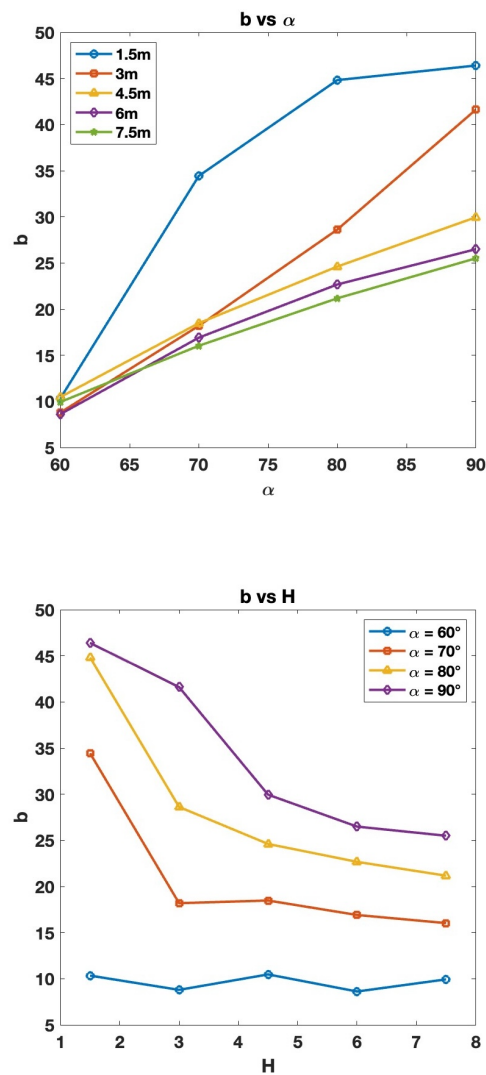


Figure 52: Comparison of the coefficient "b" for term  $Fr$  in the  $\Delta_{MIF^*}$  empirical formulae obtained by the Meta-model with degree 2 (Optimised) between  $\alpha$  and H

### Correlation of coefficient versus $\alpha$ and $h$ for the optimised $\Delta_{MIF}^*$ empirical formula 3D representation

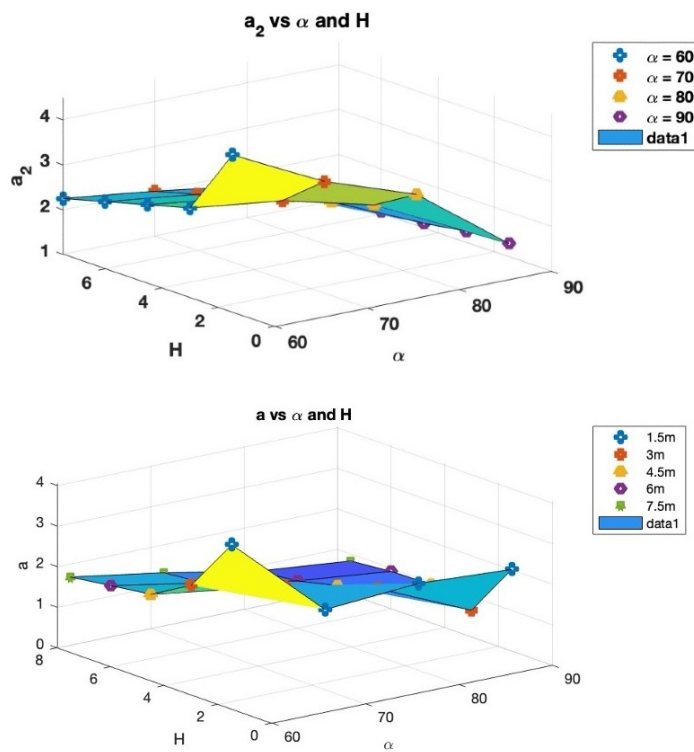


Figure 53: Comparison of the coefficients " $a_2$  and  $a$  for  $Fr^2$  term in the optimised  $\Delta_{MIF}^*$  empirical formulae with degree 2 between  $\alpha$  and  $h$  in 3D

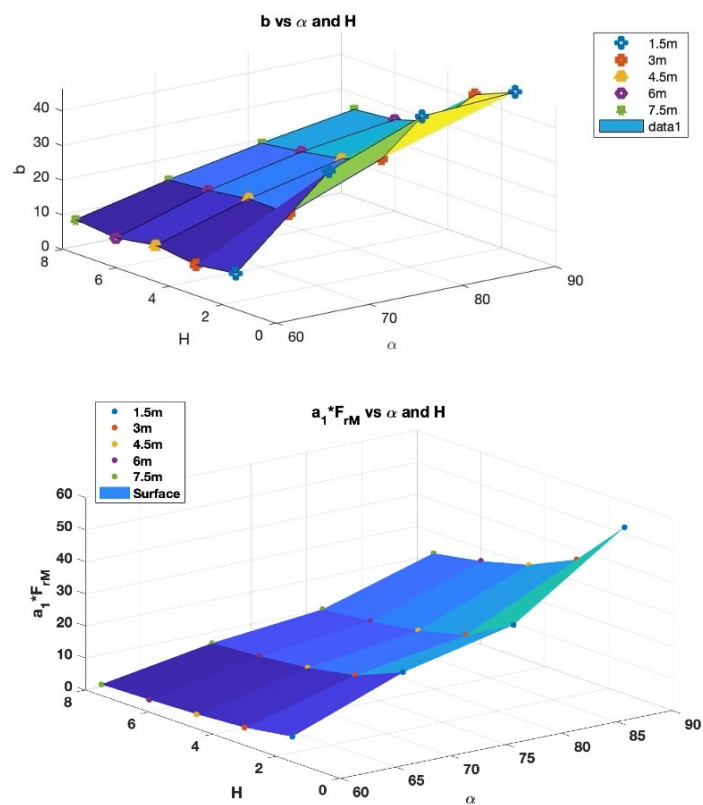


Figure 54: Comparison of the coefficients " $a_1 * F_{rM}$ " and  $b$  for  $Fr$  term in the optimised  $\Delta_{MIF}$ \* empirical formulae with degree 2 between  $\alpha$  and  $h$  in 3D



## 5 | Conclusions

In summary, the main aim of this thesis is to implementation of meta-modelling to predict maximum impact force and denormalise and calibrate the empirical formula eq.4 [13]. This empirical formula is based on polynomials eq.4, which encountered a challenge when it came to calibration. Once calibration has been achieved, the model becomes a tool for various analytical and observational purposes. In this study, instead of using interpolation between empirical formulae in different conditions, taking advantage of the meta-modelling approach leads and facilitates in order to predict the maximum impact forces. When the meta-model is created, it becomes feasible to predict the maximum impact force for any combination of velocity, front inclination, and height within the range of values used for training in the machine learning algorithm.

Polynomial Chaos Expansion (*PCE*) with six different computational methods; however 5 of the computational models can be used to obtain results with good accuracy even if the set of numerical experiments had not been designed by using probabilistic approaches such as Monte Carlo, the Meta-models have the capability of prediction of the maximum impact force with good accuracy.

The procedure of this meta-modelling is in the black-box which is not visible; therefore, due to lack of transparency, which makes it inapplicable to our demand in order to understand how the predictions are made hence, there is a need for research to uncover the working of the system and obtain the formula for prediction. Therefore, in order to obtain a new empirical formula, the Polyfit tool in MATLAB was implemented to calculate the coefficient of the empirical formula Table 14.

Furthermore, this study also investigated the impact of passive thrust  $S_p$  eq.1; by comparing Table 14 and Table 15 from an engineering point of view, it was found that passive thrust has an insignificant effect on the empirical formula; therefore, it can be disregarded.



## Bibliography

- [1] Sensitivity estimates for nonlinear mathematical models. 1(4):407–414, 1993.
- [2] M. Arattano and L. Franzi. On the evaluation of debris flows dynamics by means of mathematical models. *Natural Hazards and Earth System Sciences*, 3(6):539–544, 2003.
- [3] A. Armanini. On the dynamic impact of debris flows. *Recent developments on debris flows*, pages 208–226, 2007.
- [4] R. Barton. Metamodeling: a state of the art review. pages 237–244. IEEE. ISBN 0-7803-2109-X. doi: 10.1109/WSC.1994.717134.
- [5] E. Borgonovo. A new uncertainty importance measure. *Reliability Engineering System Safety*, 92:771–784, 6 2007. ISSN 09518320. doi: 10.1016/j.ress.2006.04.015.
- [6] L. Breiman. Random forests. *Machine Learning*, 45:5–32, 2001. ISSN 1573-0565. doi: 10.1023/A:1010933404324. URL <https://doi.org/10.1023/A:1010933404324>.
- [7] L. Bugnion, B. W. McArdell, P. Bartelt, and C. Wendeler. Measurements of hillslope debris flow impact pressure on obstacles. *Landslides*, 9:179–187, 2012.
- [8] N. C. Calhoun and J. J. Clague. Distinguishing between debris flows and hyperconcentrated flows: an example from the eastern swiss alps. *Earth Surface Processes and Landforms*, 43(6):1280–1294, 2018.
- [9] C. Calligaris, L. Zini, et al. Debris flow phenomena: a short overview. *Earth Sciences. INTECH, Croatia*, pages 71–90, 2012.
- [10] F. Calvetti. Discrete modelling of granular materials and geotechnical problems. *European Journal of Environmental and Civil Engineering*, 12:951–965, 8 2008. ISSN 1964-8189. doi: 10.1080/19648189.2008.9693055.
- [11] F. Calvetti, C. di Prisco, and R. Nova. Experimental and numerical analysis of soil–pipe interaction. *Journal of Geotechnical and Geoenvironmental Engineering*,

- 130:1292–1299, 12 2004. ISSN 1090-0241. doi: 10.1061/(ASCE)1090-0241(2004)130:12(1292).
- [12] F. Calvetti, C. di Prisco, and E. Vairaktaris. Dry granular flows impacts on rigid obstacles: Dem evaluation of a design formula for the impact force. *Procedia Engineering*, 158:290–295, 2016.
- [13] F. Calvetti, C. G. Di Prisco, and E. Vairaktaris. Dem assessment of impact forces of dry granular masses on rigid barriers. *Acta Geotechnica*, 12:129–144, 2017.
- [14] F. Calvetti, C. di Prisco, I. Redaelli, A. Sganzerla, and E. Vairaktaris. Mechanical interpretation of dry granular masses impacting on rigid obstacles. *Acta Geotechnica*, 14:1289–1305, 2019.
- [15] F. Ceccato, I. Redaelli, C. di Prisco, and P. Simonini. Impact forces of granular flows on rigid structures: Comparison between discontinuous (dem) and continuous (mpm) numerical approaches. *Computers and Geotechnics*, 103:201–217, 11 2018. ISSN 0266352X. doi: 10.1016/j.compgeo.2018.07.014.
- [16] F. Ceccato, I. Redaelli, C. di Prisco, and P. Simonini. Impact forces of granular flows on rigid structures: comparison between discontinuous (dem) and continuous (mpm) numerical approaches. *Computers and Geotechnics*, 103:201–217, 2018.
- [17] P. Coussot and M. Meunier. Recognition, classification and mechanical description of debris flows. *Earth-Science Reviews*, 40(3-4):209–227, 1996.
- [18] P. A. CUNDALL and R. D. HART. Numerical modelling of discontinua. *Engineering Computations*, 9:101–113, 2 1992. ISSN 0264-4401. doi: 10.1108/eb023851.
- [19] P. A. Cundall and O. D. L. Strack. A discrete numerical model for granular assemblies. *Géotechnique*, 29:47–65, 3 1979. ISSN 0016-8505. doi: 10.1680/geot.1979.29.1.47.
- [20] W. Dai and O. Milenkovic. Subspace pursuit for compressive sensing signal reconstruction. *IEEE Transactions on Information Theory*, 55(5):2230–2249, 2009. doi: 10.1109/TIT.2009.2016006.
- [21] T. Davies. Large debris flows: a macro-viscous phenomenon. *Acta Mechanica*, 63:161–178, 1986.
- [22] E. de Rocquigny, N. Devictor, S. Tarantola, Y. Lefebvre, N. Pérot, W. Castaings, F. Mangeant, C. Schwob, R. Lavin, J.-R. Masse, P. Limbourg, W. Kanning, and

- P. Gelder. Uncertainty in industrial practice: A guide to quantitative uncertainty management. 2 2008. doi: 10.1002/9780470770733.
- [23] P. Diaz, A. Doostan, and J. Hampton. Sparse polynomial chaos expansions via compressed sensing and d-optimal design. *Computer Methods in Applied Mechanics and Engineering*, 336:640–666, 7 2018. ISSN 00457825. doi: 10.1016/j.cma.2018.03.020.
- [24] F. Gabrieli, S. Cola, and F. Calvetti. Use of an up-scaled dem model for analysing the behaviour of a shallow foundation on a model slope. *Geomechanics and Geoengineering*, 4:109–122, 5 2009. ISSN 1748-6025. doi: 10.1080/17486020902855688.
- [25] A. Gelman, J. B. Carlin, H. S. Stern, D. B. Dunson, A. Vehtari, D. B. Rubin, J. Carlin, H. Stern, D. Rubin, and D. Dunson. Bayesian data analysis third edition (with errors fixed as of 15 february 2021), 1995.
- [26] Y. Guo and J. S. Curtis. Discrete element method simulations for complex granular flows. *Annual Review of Fluid Mechanics*, 47:21–46, 1 2015. ISSN 0066-4189. doi: 10.1146/annurev-fluid-010814-014644.
- [27] T. Hastie, R. Tibshirani, and A. Buja. Flexible discriminant analysis by optimal scoring. *Journal of the American Statistical Association*, 89:1255–1270, 12 1994. ISSN 0162-1459. doi: 10.1080/01621459.1994.10476866.
- [28] L. Highland. *Debris-flow hazards in the United States*, volume 176. US Department of the Interior, US Geological Survey, 1997.
- [29] H.-P. Huang, K.-C. Yang, and S.-W. Lai. Impact force of debris flow on filter dam. *momentum*, 9(2):03218, 2007.
- [30] J. Hübl, J. Suda, D. Proske, R. Kaitna, and C. Scheidl. Debris flow impact estimation. In *Proceedings of the 11th international symposium on water management and hydraulic engineering, Ohrid, Macedonia*, volume 1, pages 1–5. University of Ss Cyril and Methodius, Faculty of Civil Engineering, Skopje . . . , 2009.
- [31] N. Ishikawa, R. Inoue, K. Hayashi, Y. Hasegawa, and T. Mizuyama. *Experimental approach on measurement of impulsive fluid force using debris flow model*. na, 2008.
- [32] R. M. Iverson. Debris flows: behaviour and hazard assessment. *Geology Today*, 30: 15–20, 1 2014. ISSN 0266-6979. doi: 10.1111/gto.12037.
- [33] L. Jia, Z. Haijun, M. Fengshan, G. Jie, D. Xueliang, and L. Shuaiqi. Recent study sta-

- tus of debris flow in the frigid alpine mountain area in china. *Journal of Engineering Geology*, 28(S1):77–85, 2020.
- [34] J. Kaipio and E. Somersalo. Statistical inverse problems. *Journal of Computational and Applied Mathematics - J COMPUT APPL MATH*, 198:493–504, 2 2007.
- [35] R. Korlakai Vinayak and R. Gilad-Bachrach. DART: Dropouts meet Multiple Additive Regression Trees. In G. Lebanon and S. V. N. Vishwanathan, editors, *Proceedings of the Eighteenth International Conference on Artificial Intelligence and Statistics*, volume 38 of *Proceedings of Machine Learning Research*, pages 489–497, San Diego, California, USA, 09–12 May 2015. PMLR. URL <https://proceedings.mlr.press/v38/korlakaivinayak15.html>.
- [36] D. G. Krige. A statistical approach to some basic mine valuation problems on the witwatersrand, by d.g. krige, published in the journal, december 1951 : introduction by the author. *Journal of The South African Institute of Mining and Metallurgy*, 52: 201–203, 1951. URL <https://api.semanticscholar.org/CorpusID:117319434>.
- [37] S. Kucherenko, S. Tarantola, and P. Annoni. Estimation of global sensitivity indices for models with dependent variables. *Computer Physics Communications*, 183:937–946, 4 2012. ISSN 00104655. doi: 10.1016/j.cpc.2011.12.020.
- [38] J. Kwan. Supplementary technical guidance on design of rigid debris-resisting barriers, 2 2012.
- [39] S. Lambert, D. Toe, A. Mentani, and F. Bourrier. A meta-model-based procedure for quantifying the on-site efficiency of rockfall barriers. *Rock Mechanics and Rock Engineering*, 54:487–500, 2 2021. ISSN 0723-2632. doi: 10.1007/s00603-020-02298-7.
- [40] M.-J. Lee and Y.-T. Kim. Movement and deposition characteristics of debris flow according to rheological factors. *Journal of the Korean Geotechnical Society*, 29(5): 19–27, 2013.
- [41] L. Ljung. Black-box models from input-output measurements. pages 138–146. IEEE. ISBN 0-7803-6646-8. doi: 10.1109/IMTC.2001.928802.
- [42] D. Lo. *Review of natural terrain landslide debris-resisting barrier design*. Geotechnical Engineering Office, Civil Engineering Department, 2000.
- [43] S. Mallat and Z. Zhang. Matching pursuits with time-frequency dictionaries. *IEEE Transactions on Signal Processing*, 41(12):3397–3415, 1993. doi: 10.1109/78.258082.
- [44] S. Marelli and B. Sudret. *UQLab: A Framework for Uncertainty Quantifica-*

- tion in Matlab*, pages 2554–2563. doi: 10.1061/9780784413609.257. URL <https://ascelibrary.org/doi/abs/10.1061/9780784413609.257>.
- [45] G. Matheron. Principles of geostatistics. *Economic Geology*, 58:1246–1266, 12 1963. ISSN 1554-0774. doi: 10.2113/gsecongeo.58.8.1246.
- [46] Y. Pati, R. Rezaifar, and P. Krishnaprasad. Orthogonal matching pursuit: recursive function approximation with applications to wavelet decomposition. In *Proceedings of 27th Asilomar Conference on Signals, Systems and Computers*, pages 40–44 vol.1, 1993. doi: 10.1109/ACSSC.1993.342465.
- [47] I. Redaelli, C. di Prisco, and F. Calvetti. Dry granular masses impacting on rigid obstacles: numerical analysis and theoretical modelling. *Acta Geotechnica*, 16:3923–3946, 2021.
- [48] B. D. Ripley. *Pattern Recognition and Neural Networks*. Cambridge University Press, 1 1996. ISBN 9780521460866. doi: 10.1017/CBO9780511812651.
- [49] J. Sacks, W. J. Welch, T. J. Mitchell, and H. P. Wynn. Design and analysis of computer experiments. *Statistical Science*, 4, 11 1989. ISSN 0883-4237. doi: 10.1214/ss/1177012413.
- [50] P. Scotton and A. M. Deganutti. Phreatic line and dynamic impact in laboratory debris flow experiments. In *Debris-flow hazards mitigation: mechanics, prediction, and assessment*, pages 777–786. ASCE, 1997.
- [51] A. Shu, L. Wang, K. Yang, and X. Fei. Investigation on movement characteristics for non-homogeneous and solid-liquid two-phase debris flow. *Chin. Sci. Bull*, 31: 3006–3012, 2010.
- [52] J. Suda, J. Hübl, and K. Bergmeister. Design and construction of high stressed concrete structures as protection works for torrent control in the austrian alps. In *Proc. of the 3rd fib international Congress, Washington, USA*, 2010.
- [53] B. Sudret. Uncertainty propagation and sensitivity analysis in mechanical models – contributions to structural reliability and stochastic spectral methods. 2 2007.
- [54] A. Tarantola. *Inverse Problem Theory and Methods for Model Parameter Estimation*. SIAM, Jan 2005. URL [http://books.google.ie/books?id=qLSv6fpeMowC&printsec=frontcover&dq=ISBN:+978-0-89871-572-9&hl=&cd=4&source=gbs\\_api](http://books.google.ie/books?id=qLSv6fpeMowC&printsec=frontcover&dq=ISBN:+978-0-89871-572-9&hl=&cd=4&source=gbs_api).
- [55] H. Teufelsbauer, Y. Wang, S. P. Pudasaini, R. I. Borja, and W. Wu. Dem simulation

- of impact force exerted by granular flow on rigid structures. *Acta Geotechnica*, 6: 119–133, 9 2011. ISSN 1861-1125. doi: 10.1007/s11440-011-0140-9.
- [56] V. Vapnik. *The Nature of Statistical Learning Theory*. Springer Science Business Media, Jun 2013. URL [http://books.google.ie/books?id=EqgACAAAQBAJ&pg=PR5&dq=ISBN+:+978-1-4419-3160-3&hl=&cd=1&source=gbs\\_api](http://books.google.ie/books?id=EqgACAAAQBAJ&pg=PR5&dq=ISBN+:+978-1-4419-3160-3&hl=&cd=1&source=gbs_api).
- [57] Z. Wang and X. Zhang. Initiation and laws of motion of debris flow. In *Hydraulics/Hydrology of Arid Lands (H<sup>2</sup>AL)*, pages 596–601. ASCE, 1990.
- [58] S. Zhang. A comprehensive approach to the observation and prevention of debris flows in china. *Natural Hazards*, 7:1–23, 1993.

# A | Reference for figure 35

Table 17: Selective data of inputs and output parameters

$v$	$\alpha$	$h$ (m)	MIF (MN)	MIF predicted
10.805	60	1.5	3.80	3.06
12.966	60	1.5	5.26	4.81
10.805	60	3	6.96	4.91
12.966	60	3	9.80	7.45
12.966	60	4.5	12.33	15.68
17.288	60	4.5	19.73	23.59
10.805	60	6	12.09	10.99
12.966	60	6	15.30	14.85
10.805	60	7.5	13.6	14.19
12.966	60	7.5	18.8	19.57
10.805	60	1.5	3.80	3.06
12.966	60	1.5	5.26	4.81
10.805	60	3	6.96	4.91
12.966	60	3	9.80	7.45
12.966	60	4.5	12.33	15.68
17.288	60	4.5	19.73	23.59
10.805	60	6	12.09	10.99
12.966	60	6	15.3	14.85
10.805	60	7.5	13.64	14.19
12.966	60	7.5	18.86	19.57
10.805	70	1.5	4.907	7.93
12.966	70	1.5	7.103	9.62
10.805	70	3	8.553	7.14
12.966	70	3	11.21	10.83
10.805	70	4.5	13.65	14.10
12.966	70	4.5	21.426	19.53
10.805	70	7.5	19.30	17.36
12.966	70	7.5	28.09	26.74
10.805	80	1.5	7.83	8.83
12.966	80	1.5	10.71	11.42
10.805	80	4.5	19.52	20.41
12.966	80	4.5	25.99	27.06



# B | Reference for figure 36

Table 18: Prediction of MIF for new heights

$v(m/s)$	$\alpha$	$h$ (m)	MIF predicted (MN)
10.805	60	2.25	1.22
12.966	60	2.25	3.41
10.805	60	3.75	9.57
12.966	60	3.75	12.47
10.805	60	5.25	12.65
12.966	60	5.25	16.10
10.805	60	6.75	10.04
12.966	60	6.75	14.43
10.805	70	2.25	5.28
12.966	70	2.25	8.02
10.805	70	3.75	10.68
12.966	70	3.75	15.29
10.805	70	5.25	16.21
12.966	70	5.25	22.43
10.805	70	6.75	16.85
12.966	70	6.75	24.90
10.805	80	2.25	10.14
12.966	80	2.25	13.77
10.805	80	3.75	16.09
12.966	80	3.75	21.74
10.805	80	5.25	25.16
12.966	80	5.25	32.77
10.805	80	6.75	34.37
12.966	80	6.75	44.30



## List of Figures

1	DEM model initial conditions . . . . .	5
2	$\Delta_{MIF^*}$ versus $Fr$ ( $h=1.5-7.5$ )m $\alpha = 60-90$ ; Reference Mechanical parameters	7
3	3D view of the DEM model with test conditions . . . . .	8
4	Reference test results a) initial configuration of the granular mass b) final configuration of the granular mass . . . . .	9
5	Visual representation of the global theoretical framework for uncertainty quantification developed by Sudret (2007); de Rocquigny et al. (2008), which gives the theoretical foundations to the UQLAB software. . . . .	13
6	MIF versus Velocity for different conditions obtained by MATLAB Polynomial degrees 3 . . . . .	22
7	MIF versus Velocity for different conditions obtained by MATLAB Polynomial degrees 2 . . . . .	23
8	MIF versus Velocity for different conditions obtained by MATLAB Polynomial degrees 2 (Optimised) . . . . .	23
9	$\Delta_{MIF^*}$ versus $Fr$ , numerical data and interpolation (eq.4) $a= 90^\circ$ , $b= 80^\circ$ , $c=70^\circ$ , $d=60^\circ$ . . . . .	24
10	Comparison of the coefficient "a" for $v^2$ term in the optimised empirical formulae with degree 2 between $alpha$ and $h$ . . . . .	28
11	Comparison of the coefficient "b" for $v$ term in the optimised empirical formulae with degree 2 between $alpha$ and $h$ . . . . .	29
12	Comparison of the coefficient "a" for $v^2$ term in the optimised empirical formulae with degree 2 between $alpha$ and $h$ in 3D . . . . .	30
13	Comparison of the coefficient "b" for $v$ term in the optimised empirical formulae with degree 2 between $alpha$ and $h$ in 3D . . . . .	30
14	$\Delta_{MIF}$ versus Velocity for different conditions obtained by MATLAB Polynomial degrees 2 (Optimised) . . . . .	31
15	Comparison of the coefficient "a" for term $v^2$ in the $\Delta_{MIF}$ empirical formulae with degree 2 (Optimised) between $\alpha$ and $H$ . . . . .	33

16	Comparison of the coefficient "b" for term $v$ in the $\Delta_{MIF}$ empirical formulae with degree 2 (Optimised) between $\alpha$ and H . . . . .	34
17	Comparison of the coefficient "a" for $v^2$ term in the optimised $\Delta_{MIF}$ empirical formulae with degree 2 between $alpha$ and $h$ in 3D . . . . .	35
18	Comparison of the coefficient "b" for $v$ term in the optimised $\Delta_{MIF}$ empirical formulae with degree 2 between $alpha$ and $h$ in 3D . . . . .	35
19	$\Delta_{MIF}^*$ versus $Fr$ for different conditions obtained by MATLAB Polynomial degrees 2 (Optimised) . . . . .	36
20	Comparison of the coefficient "a" for term $Fr^2$ in the $\Delta_{MIF}^*$ empirical formulae with degree 2 (Optimised) between $\alpha$ and H . . . . .	38
21	Comparison of the coefficient "b" for term $Fr$ in the $\Delta_{MIF}^*$ empirical formulae with degree 2 (Optimised) between $\alpha$ and H . . . . .	39
22	Comparison of the coefficients "a" and "a <sub>2</sub> " (from eq.4) for $Fr^2$ term in the optimised $\Delta_{MIF}^*$ empirical formulae with degree 2 between $alpha$ and $h$ in 3D . . . . .	40
23	Comparison of the coefficient "b" and "a <sub>1</sub> * $Fr_M$ " (from eq.4) for $Fr$ term in the optimised $\Delta_{MIF}^*$ empirical formulae with degree 2 between $alpha$ and $h$ in 3D . . . . .	41
24	Scatter Density Plot data distribution using a defined script by author 244 (70%) input samples . . . . .	45
25	Scatter Density Plot based on Sobol series distribution using a defined script by author 244 (70%) input samples . . . . .	46
26	Scatter Density Plot based on Monte Carlo distribution using a defined script by author 244 (70%) input samples . . . . .	47
27	Scatter Density Plot based on Latin Hypercube distribution using a defined script by author 244 (70%) input samples . . . . .	48
28	PCE Histogram for different computational methods, comparison between MIF and predicted MIF . . . . .	49
29	Distribution of predicted MIF around True MIF . . . . .	49
30	Sobol' indices diagram . . . . .	52
31	First order Sobol' indices diagram for input variable parameters . . . . .	53
32	Total order Sobol' indices diagram for input variable parameters . . . . .	53
33	PCE Histogram for Bayesian, compressive between MIF and predicted MIF . . . . .	55
34	MIF predicted by meta-model versus MIF (PFC3D) . . . . .	55
35	MIF predicted by meta-model versus velocity . . . . .	56
36	MIF predicted by meta-model versus velocity for the new heights . . . . .	56

	<b>List of Figures</b>	91
37	MIF predicted by meta-model versus velocity for the new inclination . . .	57
38	MIF versus Velocity for different conditions obtained by MATLAB Polynomial degrees 2 . . . . .	58
39	MIF versus Velocity for different conditions obtained by MATLAB Polynomial degrees 3 . . . . .	58
40	MIF versus Velocity for different conditions obtained by MATLAB Polynomial degrees 2 (Optimised) . . . . .	59
41	Comparison of the coefficient "a" for $v^2$ term in the optimised empirical formulae with degree 2 between alpha and h . . . . .	62
42	Comparison of the coefficient "b" for $v$ term in the optimised empirical formulae with degree 2 between alpha and h . . . . .	63
43	Comparison of the coefficient "a" for $v^2$ term in the optimised <i>MIF</i> empirical formulae obtained by meta-model with degree 2 between <i>alpha</i> and <i>h</i> in 3D . . . . .	64
44	Comparison of the coefficient "b" for $v$ term in the optimised <i>MIF</i> empirical formulae obtained by meta-model with degree 2 between <i>alpha</i> and <i>h</i> in 3D . . . . .	64
45	$\Delta_{MIF}$ versus Velocity for different conditions obtained by MATLAB Polynomial degrees 2 (Optimised) . . . . .	65
46	Comparison of the coefficient "a" for $v^2$ term in the optimised $\Delta_{MIF}$ empirical formulae with degree 2 between <i>alpha</i> and <i>h</i> in 2D . . . . .	67
47	Comparison of the coefficient "b" for $v$ term in the optimised $\Delta_{MIF}$ empirical formulae with degree 2 between <i>alpha</i> and <i>h</i> in 2D . . . . .	68
48	Comparison of the coefficient "a" for $v^2$ term in the optimised $\Delta_{MIF}$ empirical formulae with degree 2 between alpha and h . . . . .	69
49	Comparison of the coefficient "b" for $v$ term in the optimised $\Delta_{MIF}$ empirical formulae with degree 2 between alpha and h . . . . .	69
50	$\Delta_{MIF}^*$ versus $Fr$ for different conditions obtained by MATLAB Polynomial degrees 2 (Optimised) obtained by meta-model . . . . .	70
51	Comparison of the coefficient "a" for term $Fr^2$ in the $\Delta_{MIF}^*$ empirical formulae obtained by the Meta-model with degree 2 (Optimised) between $\alpha$ and H . . . . .	72
52	Comparison of the coefficient "b" for term $Fr$ in the $\Delta_{MIF}^*$ empirical formulae obtained by the Meta-model with degree 2 (Optimised) between $\alpha$ and H . . . . .	73
53	Comparison of the coefficients "a <sub>2</sub> and a for $Fr^2$ term in the optimised $\Delta_{MIF}^*$ empirical formulae with degree 2 between <i>alpha</i> and <i>h</i> in 3D . . . .	74

- 54 Comparison of the coefficients " $a_1 * F_{rM}$ " and  $b$  for  $Fr$  term in the optimised  $\Delta_{MIF}$ \* empirical formulae with degree 2 between  $\alpha$  and  $h$  in 3D . . . . . 75

## List of Tables

1	Interpolation parameters $a_1$ and $a_2$ as a function of both front inclination and intrinsic Froude number . . . . .	8
2	Input parameters . . . . .	21
3	Empirical formula (Polynomial degrees 3) . . . . .	25
4	Empirical formula (Polynomial degrees 2) . . . . .	26
5	MIF calculated by PFC 3D optimised empirical formulae . . . . .	27
6	$\Delta_{MIF}$ versus Velocity for different conditions obtained by MATLAB Polynomial degrees 2 (Optimised) . . . . .	32
7	Normalised $\Delta_{MIF}^*$ versus $Fr$ (Optimised) . . . . .	37
8	Input parameters . . . . .	43
9	Statistical approaches for probabilistic model . . . . .	44
10	Statistical information related to different methods and errors . . . . .	50
11	. Total Sobol' indices for all the inputs . . . . .	52
12	. Total Sobol' indices for all the inputs . . . . .	54
12	$MIF$ Empirical formula for meta-model output (Polynomial degrees 3) . .	59
13	$MIF$ Empirical formula for meta-model output (Polynomial degrees 2) . .	60
14	Optimised $MIF$ Empirical formula for meta-model output (Polynomial degrees 2) . . . . .	61
15	Optimised $MIF$ Empirical formula for meta-model output (Polynomial degrees 2) . . . . .	66
16	Normalised $\Delta_{MIF}^*$ versus $Fr$ (Optimised) . . . . .	71
17	Selective data of inputs and output parameters . . . . .	85
18	Prediction of MIF for new heights . . . . .	87



## List of Symbols

Variable	Description	SI unit
$MIF$	Maximum Impact Force	MN
$S_p$	Passive thrust	MN
$\gamma_s$	weight of particle	$kN/ms$
$k_p$	??	
$\Delta_{MIF}$	dynamic contribution of impact force	MN
$\alpha$	Front inclination	Degree
$h$	Height	Meter
$v$	velocity	$m/s$
$\Delta_{MIF*}$	dynamic contribution of impact force	normalise
$\epsilon_{LOO}$	Leave-One-Out Cross-Validation	



## Acknowledgements

I would like to thank **Professor Francesco Calvetti** for supervising me through this journey of implementing these cutting-edge tools using artificial intelligence. Additionally, I am grateful to my friend **Babak Khanmohamad**, who helped me translate my abstract into Italian. Moreover, I would like to acknowledge the precious support and guidance of **Stéphane Lambert** and **Ritesh Gupta** for devoting their time, which has been instrumental in helping to comprehend meta-modelling

